Discovery of 2-(furan-2-ylmethylene)hydrazine-1-carbothioamide derivatives as novel inhibitors of SARS-CoV-2 main protease

Xiaodong Dou [a,1], Qi Sun [b,1], Guofeng Xu [a,1], Yameng Liu [a], Caifang Zhang [a], Bingding Wang [a], Yangbin Lu [b], Zheng Guo [b], Lingyu Su [a], Tongyu Huo [a], Xinyi Zhao [a], Chen Wang [a], Zhongtian Yu [b], Song Song [a], Liangren Zhang [a], Zhenming Liu [a], Luhua Lai [b,c,**], Ning Jiao [a,*]

[a] State Key Laboratory of Natural and Biomimetic Drugs, School of Pharmaceutical Sciences, Peking University, Beijing, 100191, China
[b] BNLMS, Peking-Tsinghua Center for Life Sciences at College of Chemistry and Molecular Engineering, Peking University, Beijing, 100871, China
[c] Center for Quantitative Biology, Academy for Advanced Interdisciplinary Studies, Peking University, Beijing, 100871, China

ABSTRACT

The COVID-19 posed a serious threat to human life and health, and SARS-CoV-2 M^{pro} has been considered as an attractive drug target for the treatment of COVID-19. Herein, we report 2-(furan-2-ylmethylene)hydrazine-1-carbothioamide derivatives as novel inhibitors of SARS-CoV-2 M^{pro} developed by in-house library screening and biological evaluation. Similarity search led to the identification of compound **F8–S43** with the enzymatic IC_{50} value of 10.76 μM. Further structure-based drug design and synthetic optimization uncovered compounds **F8–B6** and **F8–B22** as novel non-peptidomimetic inhibitors of M^{pro} with IC_{50} values of 1.57 μM and 1.55 μM, respectively. Moreover, enzymatic kinetic assay and mass spectrometry demonstrated that **F8–B6** was a reversible covalent inhibitor of M^{pro}. Besides, **F8–B6** showed low cytotoxicity with CC_{50} values of more than 100 μM in Vero and MDCK cells. Overall, these novel SARS-CoV-2 M^{pro} non-peptidomimetic inhibitors provide a useful starting point for further structural optimization.

1. Introduction

The outbreak of coronavirus infectious disease 2019 (COVID-19), caused by severe acute respiratory syndrome coronavirus 2 (SARS-CoV-2), has been recognized as a serious threat to human life and health [1–3]. As of March 27, 2021, the disease has caused over 480 million people infections with more than 6 million deaths globally [4]. SARS-CoV-2 is a positive-strand RNA enveloped beta-coronavirus, and similar to severe acute respiratory syndrome coronavirus (SARS-CoV) and Middle East respiratory syndrome coronavirus (MERS-CoV), containing genome encodes non-structural proteins including main protease (M^{pro}, also known as 3-chymotrypsin-like protease, $3CL^{pro}$), papain-like protease (PL^{pro}), helicase, and RNA-dependent RNA polymerase (RdRp) [5,6]. Among them, M^{pro} is a key enzyme in the viral life cycle, which is involved in the virus' replication process, and results in the maturation of at least 12 non-structural proteins [7–9]. Furthermore, the highly conserved M^{pro} in coronavirus and the absence of closely related homologs in humans make M^{pro} an attractive target for the discovery of broad-spectrum antiviral drugs [10,11].

To date, there is only one M^{pro} inhibitor on market, although a series of SARS-CoV-2 M^{pro} inhibitors have been identified (Fig. 1) [10,12]. Among them, the organoselenium derivative **1** (**Ebselen**), was first disclosed as a covalent inhibitor of SARS-CoV-2 M^{pro} by screening the approved drugs and drug candidates [13]. It is reported that **Ebselen** could inhibit SARS-CoV-2 M^{pro} activity with an IC_{50} value of 0.67 μM, and SARS-CoV-2 in Vero cells with an EC_{50} value of 4.67 μM[13]. A variety of significant peptidomimetic inhibitors of SARS-CoV-2 M^{pro} have been reported, including compound **2** (**N3**), **3** (**13b**), **4** (**11a**), **5** (**Boceprevir**), **6** (**GC-376**), **7** (**MI-09**), and **8** (**PF-07321332**), which exhibited high SARS-CoV-2 M^{pro} inhibitory activity and SARS-CoV-2 inhibition at micromolar to sub-micromolar levels [13–21]. Furthermore, **PF-07321332** was approved for mild and moderate symptoms caused by

---

SARS-CoV-2 infection by US Food and Drug Administration (FDA), and **PF-07321332** was combined with protease inhibitor and cytochrome P450 3A4 (CYP3A4) inactivator **ritonavir** to reduce its metabolism by CYP3A4 [21].

Although the peptidomimetic inhibitors are highly effective against SARS-CoV-2 M^{pro}, the stability of hydrolase limited the application of these inhibitors [21–24]. In contrast, the non-peptidomimetic inhibitors are less developed [25,26]. Su et al. and Liu et al. simultaneously reported that compound **9** (**Baicalein**) was a non-peptidomimetic inhibitor of SARS-CoV-2 M^{pro} with the enzymatic inhibitory ability and antiviral activity both at micromolar levels [27,28]. Meanwhile, compound **10**, an N-substituted isatin derivative, was identified as a potent non-peptidomimetic inhibitor of SARS-CoV-2 M^{pro}, with an IC$_{50}$ value of 0.045 μM^{29}. Furthermore, compound **11** (**Masitinib**), an orally bioavailable tyrosine kinase inhibitor, was revealed as a potent inhibitor of SARS-CoV-2 M^{pro}, with an IC$_{50}$ value of 2.50 μM, through screening a library of 1900 clinically safe drugs [30]. **Masitinib** could block the replication of coronavirus in the lungs and nose of SARS-CoV-2 infected mice [30]. Moreover, Kneller and coworkers reported that compound **12** (**HL-3-68**) exhibited SARS-CoV-2 M^{pro} inhibitory activity, with an IC$_{50}$ value of 0.29 μM, through X-ray/neutron crystallography guided drug design [31]. Additionally, compound **13** (**Jun8-76-3A**) was discovered as a non-peptidomimetic inhibitor of SARS-CoV-2 M^{pro} by the modification of known M^{pro} inhibitor **ML188** [32]. Overall, the chemical diversity of the identified non-peptidomimetic inhibitors is still highly limited. Therefore, it is urgent to develop novel non-peptidomimetic inhibitors against SARS-CoV-2 M^{pro} for the broad-spectrum antiviral drug candidate discovery, especially the new scaffold inhibitors that were not reported in previous coronavirus studies.

Herein, we report the identification of 2-(furan-2-ylmethylene)hydrazine-1-carbothioamide derivatives as novel non-peptidomimetic inhibitors of SARS-CoV-2 M^{pro} by screening our in-house library and subsequent similarity search. Interestingly, compound **F8** was disclosed with the dissociation constant (K$_D$) value of 27.7 μM, by surface plasmon resonance (SPR) assay, which also exhibited an IC$_{50}$ value of 21.28 μM by enzymatic assay. Further two-dimensional similarity search based on the structure of compound **F8** led to the identification of a series of 2-(furan-2-ylmethylene)hydrazine-1-carbothioamide derivatives as novel

SARS-CoV-2 M^{pro} inhibitors. Among them, the most potent compound, **F8–S43**, exhibited the IC$_{50}$ value of 10.76 μM against SARS-CoV-2 M^{pro}. Then, three rounds of optimization based on the structure-based drug design and synthetic modification discovered compounds **F8–B6** and **F8–B22** as non-peptidomimetic inhibitors of M^{pro} with IC$_{50}$ values of 1.57 μM and 1.55 μM, respectively. Moreover, enzymatic kinetic and mass spectrometry studies demonstrated that **F8–B6** was a reversible covalent inhibitor of M^{pro}. Besides, **F8–B6** exhibited no obvious cytotoxicity in Vero and MDCK cells with CC$_{50}$ values over 100 μM. Furthermore, the structure-activity relationship (SAR) of the newly identified scaffold was discussed, which provided useful guidance for further chemical optimization.

2. Results and discussion

2.1. Identification of novel M^{pro} inhibitors by screening in-house library

To discover novel SARS-CoV-2 M^{pro} inhibitors, especially the new chemical structures that were not previously reported in coronavirus study, an in-house library was screened by SPR assay (Fig. 2A). As drawn in Fig. 2B, compound **F8** showed the high possibility as a new inhibitor of SARS-CoV-2 M^{pro}, with the K$_D$ value of 27.7 μM. The further enzymatic assay demonstrated that compound **F8** inhibited SARS-CoV-2 M^{pro} activity with an IC$_{50}$ value of 21.28 μM (Fig. 2C). Similarity analysis of compound **F8** showed that it is not similar to any of the previously reported SARS-CoV-2 M^{pro} inhibitors with the Tanimoto coefficient below 0.14 (Fig. 2D). All of these indicated that the identified non-peptidomimetic inhibitor **F8** expanded the chemical space of SARS-CoV-2 M^{pro} inhibitors and provided a useful starting point for further structural optimization.

2.2. Similarity search and preliminary SAR study

To investigate SAR and find more potent inhibitors of this new scaffold, a two-dimensional similarity search was performed based on the chemical structure of compound **F8**. A total of 70 compounds were captured and purchased from the ChemDiv and SPECS commercial databases. As exhibited in Table 1, the replacement of the 3-carboxyl
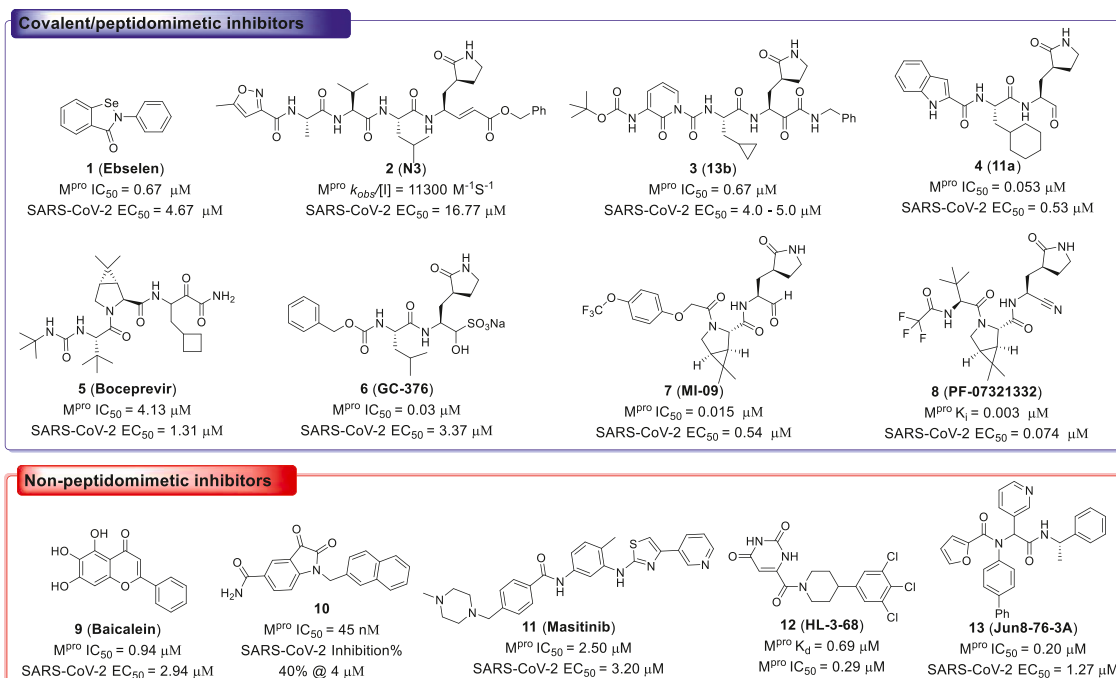

Fig. 1. Chemical structures of represented inhibitors of SARS-CoV-2 M^{pro}.
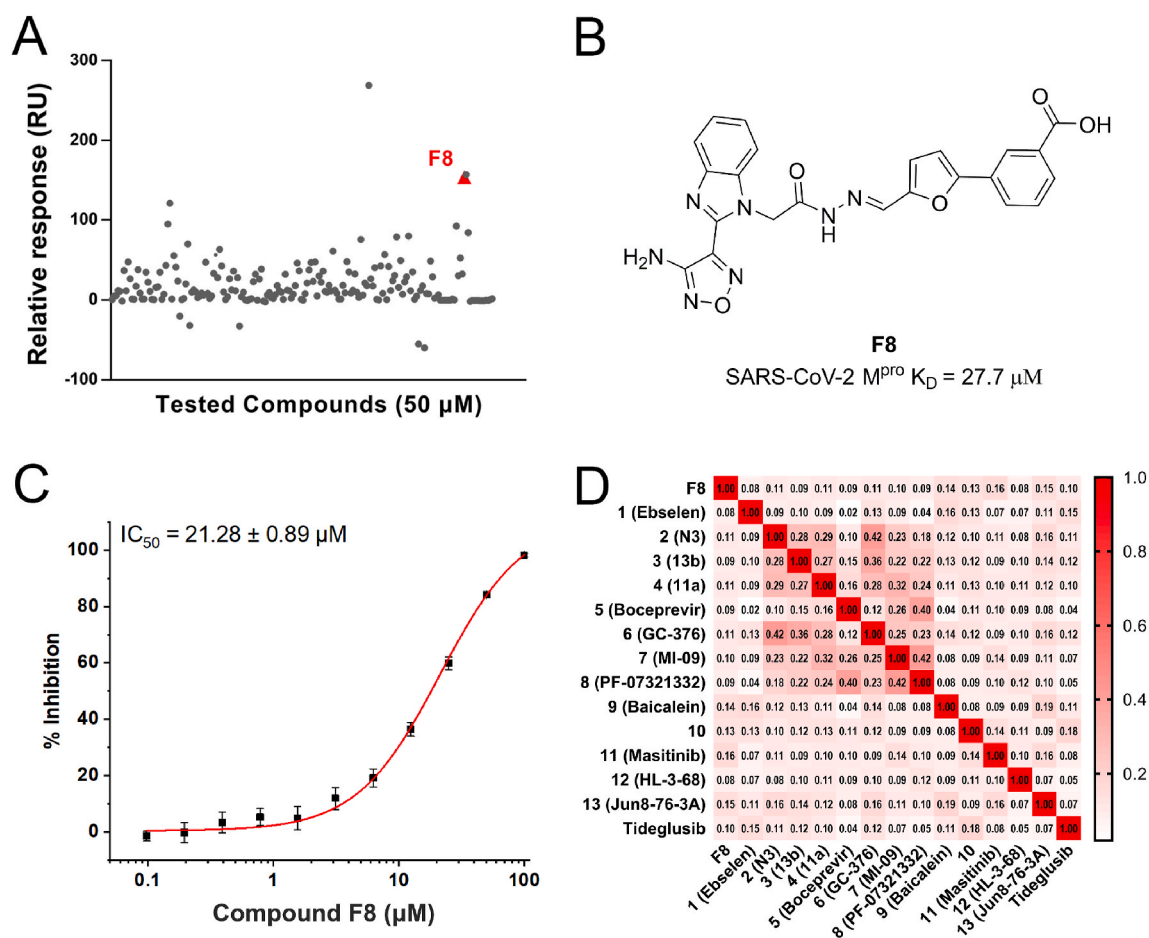
Fig. 2. The discovery of SARS-CoV-2 M^{pro} inhibitors. (A) Screen the in-house library through SPR assay. (B) The chemical structure and K$_D$ value of compound **F8**. (C) The dose-dependent curve of **F8** against SARS-CoV-2 M^{pro}. (D) The similarity analysis of compound **F8** with known SARS-CoV-2 M^{pro} inhibitors.

phenyl group of **F8** with a 3-trifluoromethyl phenyl group (**F8–S1**), a 2-carboxyl phenyl group (**F8–S2**), a 2-nitro-4-methoxy phenyl group (**F8–S3**), a 4-nitrophenyl group (**F8–S4**), a 3-methyl-4-nitrophenyl group (**F8–S5**), or a 2,3-dimethyl-4-nitrophenyl (**F8–S6**), led to a decrease of potency, indicating that the 3-carboxyl phenyl group of **F8** was essential for maintaining SARS-CoV-2 M^{pro} inhibitory activity. Furthermore, the replacement of the R^1 group of **F8** with a 10-methyl-acridin-9(10H)-one moiety (**F8–S7** to **F8–S16**), or a poly-substituted pyridine ring (**F8–S17** to **F8–S20**), the inhibitory ability of M^{pro} was decreased. Meanwhile, the replacement of the R^1 group with a 1,2,5-oxadiazol-3-amine group (**F8–S22**), or a 1-methyl-1H-tetrazol-5-amine group (**F8–S24**), produced no significant effect on inhibitory potency. Besides, the introduction of the large hydrophobic substituents group (**F8–S25**, **F8–S26**, **F8–S28** to **F8–S39**), was not conducive to the maintenance of inhibitory ability, which indicated that the R^1 group of **F8** was more suitable for small substituents. Notably, the replacement of a urea linker with a thiourea linker was likely to improve the inhibitory potency (**F8–S40** to **F8–S43**). Among them, the most potent compound, **F8–S43**, displayed an IC$_{50}$ value of 10.76 μM against SARS-CoV-2 M^{pro} (Fig. S1).

As shown in Table S1, the replacement of the thiourea linker of **F8–S43** with a hydrazine linker (**F8–S44** to **F8–S48**), an imine linker (**F8–S49** to **F8–S52**), or a double bond linker (**F8–S53** to **F8–S65**) led to the decrease of inhibitory potency, suggesting that the thiourea linker might be a good skeleton for these newly identified inhibitors. As for the right moiety of **F8**, the removal of the benzene ring resulted in the loss of potency (**F8–S66** to **F8–S70**), indicating that the benzene ring of **F8** was likely to play a hydrophobic role in the binding pocket of SARS-CoV-2

M^{pro}. As displayed in Table 2, the replacement of the 4-nitrophenyl group of **F8–S43** with a 4-bromobenzenyl group (**F8–S43–S1**), led to the remarkable loss of inhibitory activity, and the reduction of the volume of the R^1 group was beneficial to the preservation of inhibitory activity (**F8–S43–S2**, IC$_{50}$ = 8.08 μM; **F8–S43–S3**, IC$_{50}$ = 9.69 μM). Notably, the replacement of the thiourea linker to urea or guanidine linker decreased the inhibitory potency (**F8–S43–S4** to **F8–S43–S6**), indicating that the thiourea linker was very important for the maintenance and improvement of the potency. To study the SAR of the right moiety, the hydrophobic substituent of the left moiety and the thiourea linker were fixed according to the structure of **F8–S43**. As drawn in Table S2, the decrease of the hydrophobic volume of the right moiety was not conducive to the maintenance of activity (**F8–S43–S11** to **F8–S43–S32**). All in all, these results indicate that the newly identified scaffold expanded the chemical diversity of SARS-CoV-2 M^{pro} inhibitors, which could serve as a starting point for subsequent structural optimization.

2.3. Rational design and synthetic optimization

2.3.1. Structure-based design of newly identified scaffold

To guide the structural optimization of the newly identified scaffold, the representative compound **F8–S43** was docked into the catalytic site of the SARS-CoV-2 M^{pro} (PDB ID, 7JU7) [30]. As shown in Fig. 3A, compound **F8–S43** was embedded into the catalytic site of SARS-CoV-2 M^{pro} and occupied the S1 and S2 sites, while the S1′, S3, and S4 sites were not filled with **F8–S43**. Furthermore, the 4-nitrophenyl moiety of **F8–S43** was located at the S1 site and formed a hydrogen bond with

Table 1

The chemical structures and enzymatic activities of the 43 analogs of **F8**.

Left moiety — R¹ / NH / N / O / R² — Right moiety

Compounds	R [1]	X	R [2]	Inhibition % (50 μM) [a]	IC$_{50}$ ± SD (μM) [a]
Tideglusib	–	–	–	98.6	0.30 ± 0.02
F8	(structure)	O	(COOH-aryl)	65.0	21.28 ± 0.89
F8–S1	(structure)	O	(CF$_3$-aryl)	25.5	N.T. [b]
F8–S2	(structure)	O	(HOOC-aryl)	41.7	N.T.
F8–S3	(structure)	O	(O$_2$N, OMe-aryl)	<20.0	N.T.
F8–S4	(structure)	O	(NO$_2$-aryl)	30.1	N.T.
F8–S5	(structure)	O	(NO$_2$-aryl)	42.9	N.T.
F8–S6	(structure)	O	(NO$_2$-aryl)	<20.0	N.T.
F8–S7	(structure)	O	(phenyl)	21.3	N.T.
F8–S8	(structure)	O	(NO$_2$-aryl)	26.8	N.T.
F8–S9	(structure)	O	(COOH, OH-aryl)	54.5	N.T.
F8–S10	(structure)	O	(NO$_2$-aryl)	55.4	N.T.
F8–S11	(structure)	O	(NO$_2$-aryl)	22.5	N.T.
F8–S12	(structure)	O	(NO$_2$, Cl-aryl)	<20.0	N.T.
F8–S13	(structure)	O	(COOEt-aryl)	<20	N.T.
F8–S14	(structure)	O	(NO$_2$-aryl)	30.0	N.T.
F8–S15	(structure)	O	(Cl, NO$_2$-aryl)	24.1	N.T.

Table 1 (*continued*)

Compounds	R [1]	X	R [2]	Inhibition % (50 μM) [a]	IC$_{50}$ ± SD (μM) [a]
F8–S16	(structure)	O	(OMe, NO$_2$-aryl)	26.0	N.T.
F8–S17	(structure)	O	(COOH-aryl)	37.3	N.T.
F8–S18	(structure)	O	(COOH-aryl)	36.2	N.T.
F8–S19	(structure)	O	(COOH-aryl)	32.9	N.T.
F8–S20	(structure)	O	(COOH, Cl-aryl)	38.3	N.T.
F8–S21	(structure)	O	(NO$_2$-aryl)	31.2	N.T.
F8–S22	(structure)	O	(O$_2$N, Cl-aryl)	70.9	25.02 ± 1.11
F8–S23	(structure)	O	(HOOC-aryl)	34.5	N.T.
F8–S24	(structure)	O	(O$_2$N-aryl)	86.0	17.50 ± 1.65
F8–S25	(structure)	O	(HOOC-aryl)	45.3	N.T.
F8–S26	(structure)	O	(NO$_2$, Cl-aryl)	22.4	N.T.
F8–S27	(structure)	O	(COOH-aryl)	29.4	N.T.
F8–S28	(structure)	O	(COOH-aryl)	44.6	N.T.
F8–S29	(structure)	O	(COOH-aryl)	33.7	N.T.
F8–S30	(structure)	O	(COOH-aryl)	35.1	N.T.
F8–S31	(structure)	O	(COOH, Cl-aryl)	35.8	N.T.
F8–S32	(structure)	O	(NO$_2$-aryl)	24.2	N.T.
F8–S33	(structure)	O	(NO$_2$, Cl-aryl)	<20.0	N.T.
F8–S34	(structure)	O	(NO$_2$-aryl)	<20.0	N.T.
F8–S35	(structure)	O	(NO$_2$-aryl)	62.8	N.T.
F8–S36	(structure)	O	(NO$_2$-aryl)	23.3	N.T.
F8–S37	(structure)	O	(NO$_2$-aryl)	<20.0	N.T.

Table 1 (*continued*)

Compounds	R [1]	X	R [2]	Inhibition % (50 μM) [a]	IC$_{50}$ ± SD (μM) [a]
F8-S38	(naphthyl-CH(CH$_3$)-NH-)	O	(4-nitrophenyl)	23.0	N.T.
F8-S39	(2-HO-phenyl-CH=CH-C(CH$_3$)-NH-C(=O)-)	O	(4-nitrophenyl)	38.3	N.T.
F8-S40	H$_2$N–	S	(COOH-phenyl)	85.1	10.88 ± 0.16
F8-S41	(CH$_2$=CH-CH(CH$_3$)-NH-)	S	(4-nitrophenyl)	51.4	N.T.
F8-S42	(benzyl-NH-)	S	(CH$_3$, COOH-phenyl)	55.9	N.T.
F8-S43	(1,5-dimethyl-2-phenyl-pyrazol-3-one-4-yl-NH-)	S	(4-nitrophenyl)	95.0	10.76 ± 0.48

[a] Data are presented as geometric mean values of at least two independent runs.

[b] Not tested.

His163, and the furan ring was deeply buried in the S2 site and had a π-π stacking interaction with the imidazole of His41 (Fig. 3B and Fig. S2). Meanwhile, the thiourea linker of **F8-S43** formed two hydrogen bonds to the backbone carbonyl of Cys44, so the removal or replacement of the thiourea linker led to the loss of inhibitory ability. Besides, the right moiety of **F8-S43** was located at the solvent-exposed area and formed a hydrogen bond with Ser46. As drawn in Fig. 3C, the removal of the dihydro-2*H*-pyrazol-2′-one moiety of **F8-S43** had no impact on enzymatic inhibition in the aforementioned similarity search study, so the solvent-exposed region of this scaffold was structurally modified to improve the inhibitory potency of SARS-CoV-2 M^{pro}, followed by S1 and S2 pockets occupied moieties.
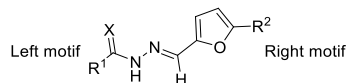
2.3.2. Synthesis of target compounds

The target compounds **F8-A1** to **F8-A9** were synthesized as illustrated in Scheme 1. Briefly, we synthesized the intermediates (**15**) from appropriate aryl boronic acid (**14**) with 5-bromofuran-2-carbaldehyde through Pd(PPh$_3$)$_4$ catalyzed Suzuki-Miyaura cross-coupling reaction [33]. Then, corresponding intermediates (**15**) reacted with substituted thiosemicarbazide to produce imine linkage (**F8-A1** to **F8-A9**) through modification of published procedures or known methods [34,35].

The synthetic routes of the target compounds **F8-B1** to **F8-B13** were described in Scheme 2. The building blocks (**17** and **19**) were prepared following previously described procedures [33]. Shortly, the starting
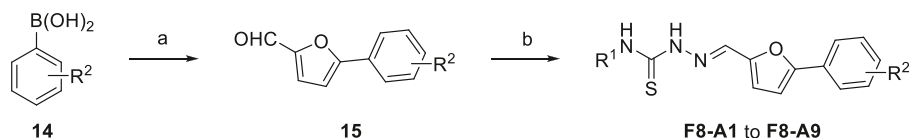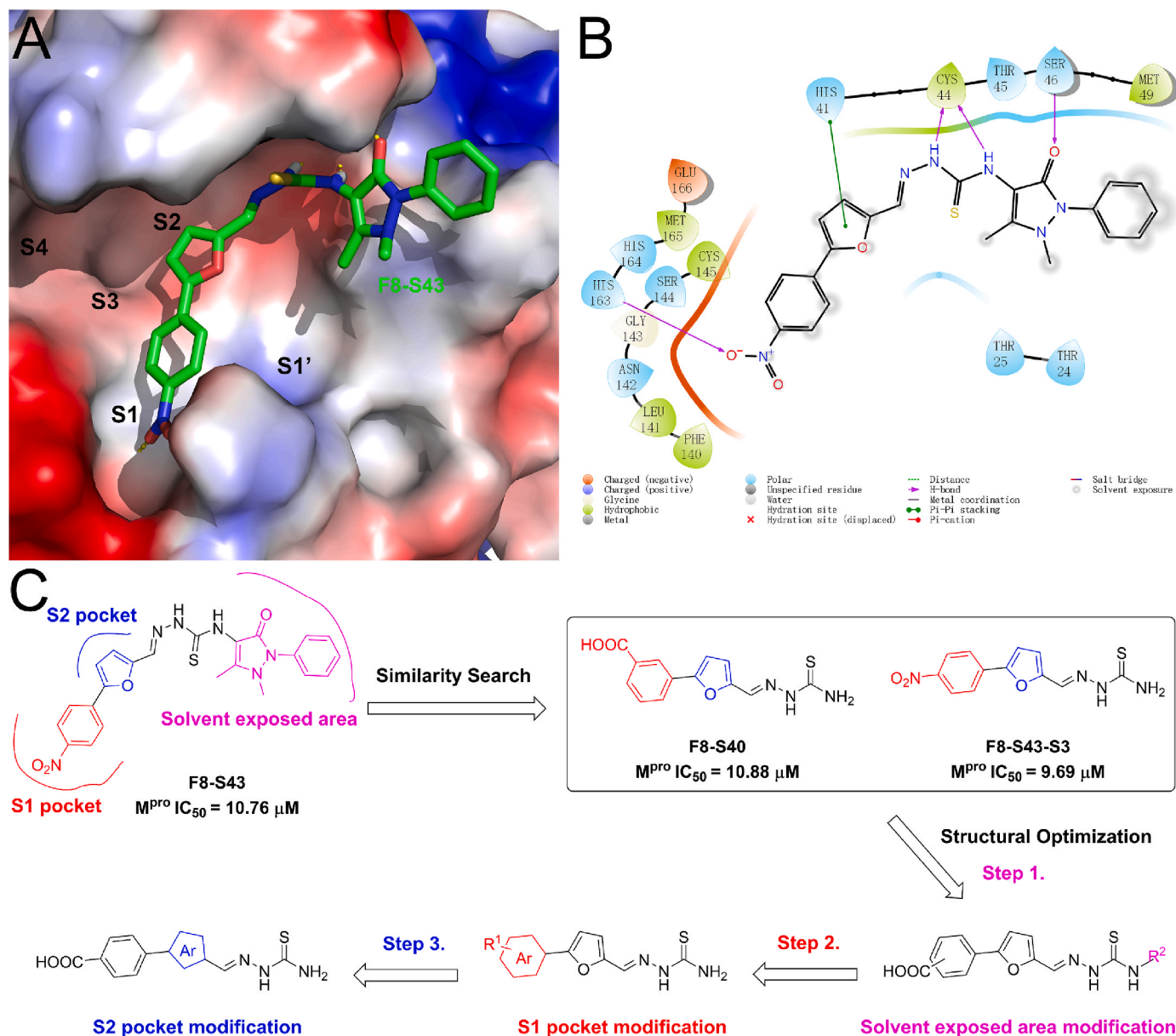
Table 2

The chemical structures and enzymatic activities of the 10 analogs of **F8-S43**.

Left motif R^1-C(=X)-NH-N=CH-(furan)-R^2 Right motif

Compounds	R [1]	X	R [2]	Inhibition% (50 μM) [a]	IC$_{50}$ ± SD (μM) [a]
Tideglusib	–	–	–	98.6	0.30 ± 0.02
F8-S43	(1,5-dimethyl-2-phenyl-pyrazol-3-one-4-yl-NH-)	S	(4-NO$_2$-phenyl)	95.0	10.76 ± 0.48
F8-S43-S1	(1,5-dimethyl-2-phenyl-pyrazol-3-one-4-yl-NH-)	S	(4-Br-phenyl)	27.7	N.T. [b]
F8-S43-S2	NH$_2$	S	(3-NO$_2$-phenyl)	81.6	8.08 ± 0.38
F8-S43-S3	NH$_2$	S	(4-NO$_2$-phenyl)	81.1	9.69 ± 0.45
F8-S43-S4	NH$_2$	O	(4-NO$_2$-phenyl)	<20.0	N.T.
F8-S43-S5	(O$_2$N-NH-NH-)	NH	(2-NO$_2$,4,5-dimethyl-phenyl)	20.1	N.T.
F8-S43-S6	(O$_2$N-NH-NH-)	NH	(2-NO$_2$,4,6-dimethyl-phenyl)	28.7	N.T.
F8-S43-S7	(CH$_2$=CH-CH$_2$-NH-)	S	(2-NO$_2$-phenyl)	28.4	N.T.
F8-S43-S8	(CH$_2$=CH-CH$_2$-NH-)	S	(3,5-di-COOH-phenyl)	34.2	N.T.
F8-S43-S9	(1,1-dioxo-thiolan-3-yl-NH-)	S	(3-NO$_2$-phenyl)	30.2	N.T.
F8-S43-S10	(phenyl-NH-)	S	(3-NO$_2$-phenyl)	<20.0	N.T.

[a] Data are presented as geometric mean values of at least two independent runs.

[b] Not tested.

Fig. 3. Predicted binding mode of compound **F8–S43**. (A) The binding pattern of compound **F8–S43** with SARS-CoV-2 M^{pro} in surface and 2D diagram (B). Hydrogen bonds are represented by yellow lines. Images depicting the proposed binding modes were generated using PyMOL software. (C) The design of newly identified SARS-CoV-2 M^{pro} inhibitors.

F8-A1, R^1 = H, R^2 = 3-carboxyl
F8-A2, R^1 = H, R^2 = 4-carboxyl
F8-A3, R^1 = methyl, R^2 = 3-carboxyl
F8-A4, R^1 = methyl, R^2 = 4-carboxyl
F8-A5, R^1 = 4-chlorophenyl, R^2 = 3-carboxyl

F8-A6, R^1 = 4-chlorophenyl, R^2 = 4-carboxyl
F8-A7, R^1 = 3-trifluoromethylphenyl, R^2 = 3-carboxyl
F8-A8, R^1 = 3-trifluoromethylphenyl, R^2 = 4-carboxyl
F8-A9, R^1 = *N*-cyclohexyl, R^2 = 4-carboxyl

Scheme 1. Synthetic Route of Compounds **F8-A1** to **F8-A9**. Reagents and conditions: (a) 5-bromofuran-2-carbaldehyde, Pd(PPh$_3$)$_4$, K$_2$CO$_3$, PhMe/EtOH/H$_2$O, 90 °C, overnight; (b) R^{1}NH$_2$CSNHNH$_2$, MeOH, 50 °C, 4 h.
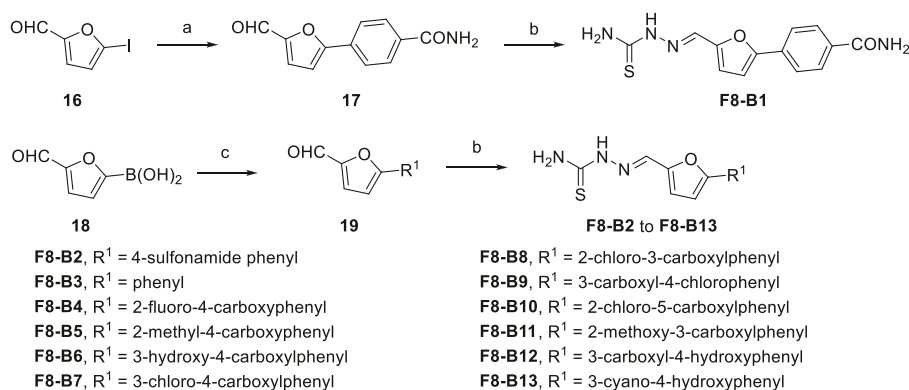
Scheme 2. Synthetic Route of Compounds **F8–B1** to **F8–B13**. Reagents and conditions: (a) (4-carbamoylphenyl)boronic acid, Pd(PPh₃)₄, K₂CO₃, PhMe/EtOH/H₂O, 90 °C, overnight; (b) Thiosemicarbazide, MeOH, 50 °C, 4 h; (c) Substituted bromobenzene, Pd(PPh₃)₂Cl₂, Na₂CO₃, MeCN/H₂O, 90 °C, overnight; or substituted bromobenzene, Pd(PPh₃)₄, K₂CO₃, PhMe/EtOH/H₂O, 90 °C, overnight; or Substituted bromobenzene, Pd(PPh₃)₂Cl₂, 2 M Na₂CO₃, DME/EtOH, 60 °C, overnight.

material 5-iodofuran-2-carbaldehyde (**16**) or (5-formylfuran-2-yl) boronic acid (**18**) reacted with (4-carbamoylphenyl)boronic acid or substituted bromobenzene to form corresponding intermediates (**17** and **19**) through Suzuki-Miyaura cross-coupling reaction. Then, the aldehyde group of intermediates (**17** and **19**) condensed with the amino group of thiosemicarbazide to form the target compounds (**F8–B1** to **F8–B13**).

As drawn in Scheme 3, the synthetic methods of **F8–B14** to **F8–B21** were similar to the aforementioned synthesis of compounds **F8–B1** to **F8–B13**. Simply, 5-bromofuran-2-carbaldehyde (**20**) reacted with corresponding aryl boronic acid to form intermediates (**21**), then the newly prepared intermediates condensed with thiosemicarbazide to give target compounds **F8–B14** to **F8–B21**. Moreover, the intermediate (**23**), 5-benzylfuran-2-carbaldehyde, was synthesized by the starting material 5-(hydroxymethyl)furan-2-carbaldehyde (**22**) reacted with benzene through substitution reaction following previously described procedures [36]. Then, the intermediate (**23**) was condensed with thiosemicarbazide to give the target compound **F8–B22**.

As shown in Scheme 4, the synthetic methods of **F8–C1** to **F8–C4** were similar to the aforesaid synthesis of compounds **F8–B1** to **F8–B13**. Briefly, the appropriate aryl bromides (**24**) reacted with (4-carbamoyl-phenyl)boronic acid to form intermediates (**25**) through Suzuki-Miyaura cross-coupling reaction. Then, the corresponding intermediates condensed with thiosemicarbazide to give target compounds **F8–C1** to **F8–C4**. All of the synthesized target compounds were characterized by ¹H NMR, ¹³C NMR, and high-resolution mass spectrometry (HRMS) experiments as single substances.

2.3.3. Biological evaluation and SAR study

The synthesized target compounds were evaluated through aforesaid enzymatic assay, and the results were summarized in Table 3. To investigate the SAR of the solvent-exposed region of the newly identified scaffold, the other regions were fixed with the same substituents. Notably, with the replacement of the 3-carboxyl phenyl group of **F8-A1** with a 4-carboxyl phenyl group (**F8-A2**), the inhibitory potency was maintained. Furthermore, the introduction of hydrophobic substituents, including methyl, 4-chlorophenyl, 3-trifluoromethyl phenyl, and cyclohexyl amino groups (**F8-A3 to F8-A9**), led to decreased inhibitory ability. Thus, the R¹ group of this scaffold was fused with a hydrogen atom, and the R² group was further structural modified to enhance the inhibitory ability and explore explicit SAR.

As for the phenyl moiety of the newly identified scaffold (Table 4), the replacement of 4-carboxyl phenyl group of **F8-A2** with a 4-amide phenyl group (**F8–B1**), a 4-sulfonyl phenyl group (**F8–B2**), or a phenyl group (**F8–B3**), resulted in moderate improve in inhibitory activity. When the benzene ring had multiple substituents (**F8–B4** to **F8–B14**), the polar substituents, including carboxyl group, hydroxyl group, and methoxy group, were favorable to maintain or promote the inhibitory ability. Among them, the 3-hydroxy-4-carboxyl phenyl group substituted compound **F8–B6** exhibited good activity, with the IC₅₀ value of 1.57 μM (Fig. S1). Whereas the replacement of the 4-carboxyl phenyl group of **F8-A2** with a 3, 4-dichlorobenzyl group (**F8–B15**), led to the loss of inhibitory potency, which meant that the phenyl moiety of the newly identified scaffold was not suitable to be replaced by a completely hydrophobic substituent. Furthermore, this moiety was
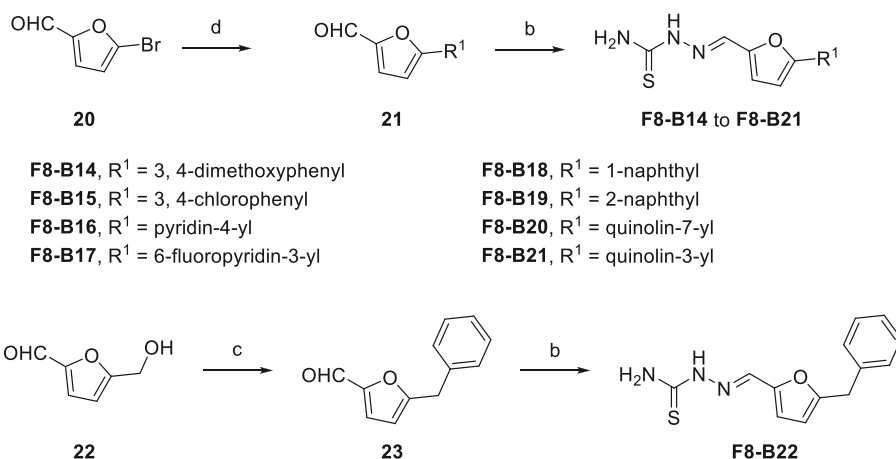

Scheme 3. Synthetic Route of Compounds **F8–B14** to **F8–B22**. Reagents and conditions: (a) Corresponding aryl boronic acid, Pd(PPh₃)₄, K₂CO₃, PhMe/EtOH/H₂O, 90 °C, overnight; (b) Thiosemicarbazide, MeOH, 50 °C, 4 h; (c) benzene, trifluoromethanesulfonic acid, r.t.
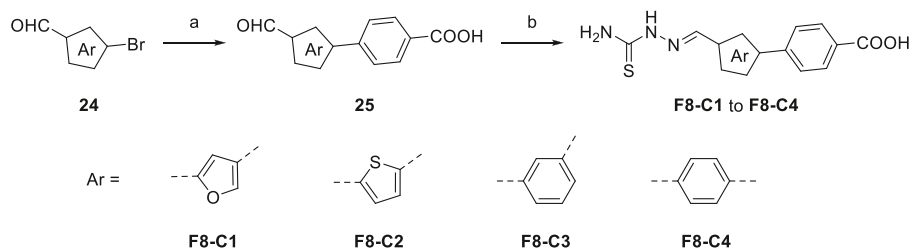
Scheme 4. Synthetic Route of Compounds **F8–C1** to **F8–C4**. Reagents and conditions: (a) (4-carbamoylphenyl)boronic acid, Pd(PPh$_3$)$_4$, K$_2$CO$_3$, PhMe/EtOH/H$_2$O, 90 °C, overnight; (b) Thiosemicarbazide, MeOH, 50 °C, 4 h.

Table 3
The chemical structures and enzymatic activities of **F8-A1** to **F8-A9**.
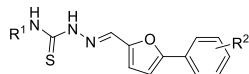
Compounds	R [1]	R [2]	Inhibition% (50 μM) [a]	IC$_{50}$ ± SD (μM) [a]
F8-A1 (F8–S40)	H	3-COOH	85.1	10.88 ± 0.16
F8-A2	H	4-COOH	89.4	17.53 ± 3.98
F8-A3	Me	3-COOH	22.2	N.T. [b]
F8-A4	Me	4-COOH	39.5	N.T.
F8-A5	Cl	3-COOH	43.8	N.T.
F8-A6	Cl	4-COOH	27.5	N.T.
F8-A7	F$_3$C	3-COOH	43.0	N.T.
F8-A8	F$_3$C	4-COOH	38.6	N.T.
F8-A9	cyclohexyl-NH	4-COOH	37.3	N.T.

[a] Data are presented as geometric mean values of at least two independent runs.
[b] Not tested.

compatible with pyridine or substituted pyridine rings (**F8–B16** to **F8–B17**). Intriguingly, the naphthalene ring substitution was not conducive to the preservation of inhibitory activity (**F8–B18** to **F8–B19**), while the quinoline ring did not affect the potency (**F8–B20** to **F8–B21**). Therefore, the aforementioned moiety might be more suitable for nitrogen heterocyclic replacement. Notably, the replacement of the 4-carboxyl phenyl group of **F8-A2** with a benzyl group (**F8–B22**), led to the enhancement of potency, and the compound **F8–B22** displayed an IC$_{50}$ value of 1.55 μM (Fig. S1), which potency was 13-fold more than the initial compound **F8**.
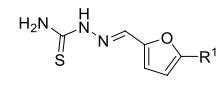
To investigate the furan ring moiety of the newly identified scaffold, the benzene ring moiety was designed to fix with the benzyl group, as the compound **F8–B22** displayed an IC$_{50}$ value of 1.55 μM. However, the designed compounds were difficult to synthesize, so the furan ring moiety was optimized with the 4-carboxyl phenyl group replacement. As drawn in Table 5, the replacement of 2,5-position substituted furan ring of **F8-A2** with a 2,4-position substituted furan ring (**F8–C1**), a 2,5-position substituted thiophene ring (**F8–C2**), or a 1,3-position substituted benzene ring (**F8–C3**), let to maintain or improve inhibitory potency.
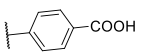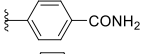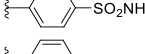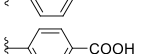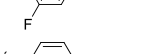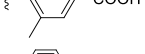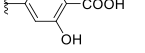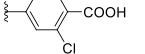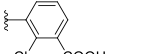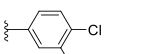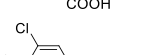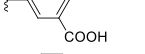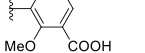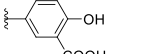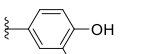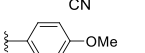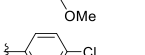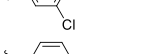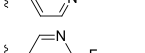
Whereas, the 1,4-position substituted benzene ring (**F8–C4**) was not conducive to the preservation of inhibitory activity, indicating that the furan ring moiety acted as an important connecting linker and prefer to three atomic lengths. It is noteworthy that the introduction of a substituent to the furan, thiophene, or benzene ring might be beneficial to the improvement of activity, however the synthesis was too difficult to achieve. Thus, we are trying to perform scaffold hopping based on this scaffold to improve the synthetic accessibility and inhibitory potency in the future.

Meanwhile, the mechanism of action of these newly identified inhibitors was investigated through enzymatic kinetic and mass spectrometry assays. As exhibited in Fig. 4A and B, the Lineweaver-Burk plot with different **F8–B6** concentrations yielded an intercept at the *X*-axis, indicating that **F8–B6** is a non-competitive inhibitor of SARS-CoV-2 M^{pro}. Moreover, prolonged incubation of SARS-CoV-2 M^{pro} with **F8–B6** exhibited a time-dependent increase of inhibition activity (Figs. S3A–3C). The addition of dithiothreitol (DTT) could reverse the inhibitory effect of **F8–B6** (Fig. S3D). Further liquid chromatography-tandem mass spectrometry (LC-MS/MS) analysis demonstrated that **F8–B6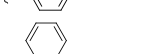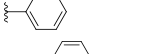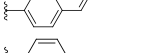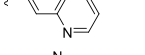** covalently bonded to SARS-CoV-2 M^{pro} (Fig. 4C), which was similar to the previously reported covalent inhibitor **Ebselen** [13], with more than one **F8–B6** can be covalently bonded to the dimer of M^{pro}. Notably, thiacetazone moiety was identified as a covalent warhead to cystine in previous work [37,38], and this was consistent with the above SAR that the introduction of thiacetazone moiety led to the increase of inhibitory activity. However, the specific covalent mechanism still needed to be further studied. In addition, reversibility assay of **F8–B6** to SARS-CoV-2 M^{pro} revealed that the ultrafiltration of inhibitor could recover enzymatic activity to a certain extent (Fig. 4D), which indicated that **F8–B6** is a reversible inhibitor. Overall, the enzymatic kinetic and mass spectrometry studies demonstrated that **F8–B6** is a reversible covalent inhibitor of SARS-CoV-2 M^{pro}. Interestingly, during the review process of this manuscript, Xu and coworkers reported that thiosemicarbazone is a promising scaffold for the inhibition of SARS-CoV-2 M^{pro} activity [39]. Besides, thiosemicarbazones are also well-known inhibitors of human Cathepsins. Pandey and coworkers reported that thiosemicarbazones derivatives are inhibitors of Cathepsin B, H, and L through a multi-target approach [40]. Notably, Cathepsin L is a key host cysteine protease utilized by coronaviruses for cell entry and is a promising drug target for novel antivirals against [41,42]. Thus, the selectivity of compounds **F8–B6** and **F8–B22** against Cathepsin L was investigated through previously reported method [43], and the results demonstrated that compounds **F8–B6** and **F8–B22** exhibited moderate inhibition of Cathepsin L, with the IC$_{50}$ values of 16.33 μM and 8.09 μM, respectively (Fig. S4).

Meanwhile, two compounds **F8–B6** and **F8–B22**, with good SARS-CoV-2 M^{pro} inhibitory abilities, were further evaluated for their cytotoxic activities in Vero and MDCK cells by MTT assay. As drawn in Fig. 5A and B, both compounds **F8–B6** and **F8–B22** exhibited low cytotoxicity, and **F8–B6** showed the CC$_{50}$ values more than 100 μM in Vero and MDCK cells, while **F8–B22** displayed the CC$_{50}$ values around 100 μM in Vero cells, and above 100 μM in MDCK cells.

Table 4
The chemical structures and enzymatic activities of **F8–B1** to **F8–B22**.
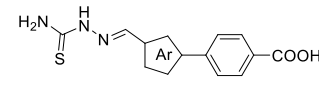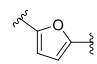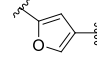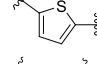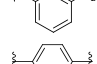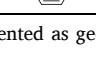

Compounds	R [1]	Inhibition% (50 μM) [a]	IC$_{50}$ ± SD (μM) [a]
F8–A2	⟶COOH	89.4	17.53 ± 3.98
F8–B1	⟶CONH$_2$	94.2	4.00 ± 0.25
F8–B2	⟶SO$_2$NH$_2$	98.5	5.39 ± 0.14
F8–B3	(phenyl)	100.0	4.05 ± 0.26
F8–B4	⟶COOH, F	100.6	8.14 ± 1.14
F8–B5	⟶COOH, CH$_3$	98.5	4.69 ± 0.34
F8–B6	⟶COOH, OH	102.2	1.57 ± 0.08
F8–B7	⟶COOH, Cl	89.0	32.53 ± 2.33
F8–B8	Cl, COOH	84.4	40.59 ± 1.06
F8–B9	Cl, COOH	93.6	25.39 ± 2.05
F8–B10	Cl, COOH	97.2	10.0 ± 0.50
F8–B11	MeO, COOH	79.8	N.T. [b]
F8–B12	OH, COOH	114.8	9.09 ± 1.05
F8–B13	OH, CN	106.6	4.14 ± 0.16
F8–B14	OMe, OMe	102.5	5.81 ± 0.07
F8–B15	Cl, Cl	49.8	N.T.
F8–B16	(pyridine N)	95.4	7.09 ± 0.51
F8–B17	(pyridine N, F)	97.4	8.76 ± 0.75
F8–B18	(naphthalene)	73.2	N.T.
F8–B19	(naphthalene)	54.1	N.T.
F8–B20	(quinoline N)	92.3	10.40 ± 2.20
F8–B21	(quinoline N)	88.9	10.30 ± 0.70
F8–B22	(benzyl)	100.1	1.55 ± 0.08

[a] Data are presented as geometric mean values of at least two independent runs.
[b] Not tested.

Table 5
The chemical structures and enzymatic activities of **F8–C1** to **F8–C4**.

Compounds	Ar	Inhibition% (50 μM) [a]	IC$_{50}$ ± SD (μM) [a]
F8–A2	(furan)	89.4	17.53 ± 3.98
F8–C1	(furan)	90.9	24.56 ± 0.70
F8–C2	(thiophene)	95.1	5.78 ± 0.30
F8–C3	(benzene 1,3)	99.2	5.44 ± 0.16
F8–C4	(benzene 1,4)	64.0	N.T. [b]

[a] Data are presented as geometric mean values of at least two independent runs.
[b] Not tested.

3. Conclusion

In the current work, a series of 2-(furan-2-ylmethylene)hydrazine-1-carbothioamide derivatives were identified as non-peptidomimetic inhibitors of SARS-CoV-2 M^{pro} through screening an in-house library by SPR and enzymatic assays. Further similarity search led to the identification of compound **F8–S43**, which exhibited an IC$_{50}$ value of 10.76 μM against SARS-CoV-2 M^{pro}. Then, three rounds of optimization based on the structure-based drug design and synthetic modification discovered compounds **F8–B6** and **F8–B22** as non-peptidomimetic inhibitors of M^{pro} with IC$_{50}$ values of 1.57 μM and 1.55 μM, respectively. Moreover, enzymatic kinetic and mass spectrometry analysis demonstrated that **F8–B6** was a reversible covalent inhibitor of M^{pro}. Besides, **F8–B6** displayed no obvious cytotoxicity in Vero and MDCK cells. Taken together, this chemical series may serve as a good starting point for the further optimization of SARS-CoV-2 M^{pro} non-peptidomimetic inhibitors.

4. Experimental section

4.1. Chemistry

General method. Synthesis reagents and solvents were obtained from commercial suppliers and used without further purification. Characterizations of compounds are provided in the Supporting Information. ^{1}H and ^{13}C NMR spectra were recorded on Bruker (400 MHz) instruments, using dimethyl sulfoxide (DMSO-d_6) as solvents. Chemical shifts are given in parts per million (ppm) downfield from tetramethylsilane (δ) as the internal standard in deuterated solvent and coupling constants (J) are in Hertz (Hz). Data are reported as follows: chemical shift, integration, multiplicity (s = singlet, d = doublet, t = triplet, q = quartet, dd = doublet of doublet, ddd = doublet of doublet of doublet, dt = doublet of triplet, m = multiplet, bs = broad signal), and coupling constants. High-resolution mass spectra were recorded on a Bruker Apex IV FTMS mass spectrometer using electrospray ionization (ESI). All compounds tested in biological assays were >95% pure.

4.1.1. General procedure A

A schlenk tube was charged with 5-bromofuran-2-carbaldehyde (1
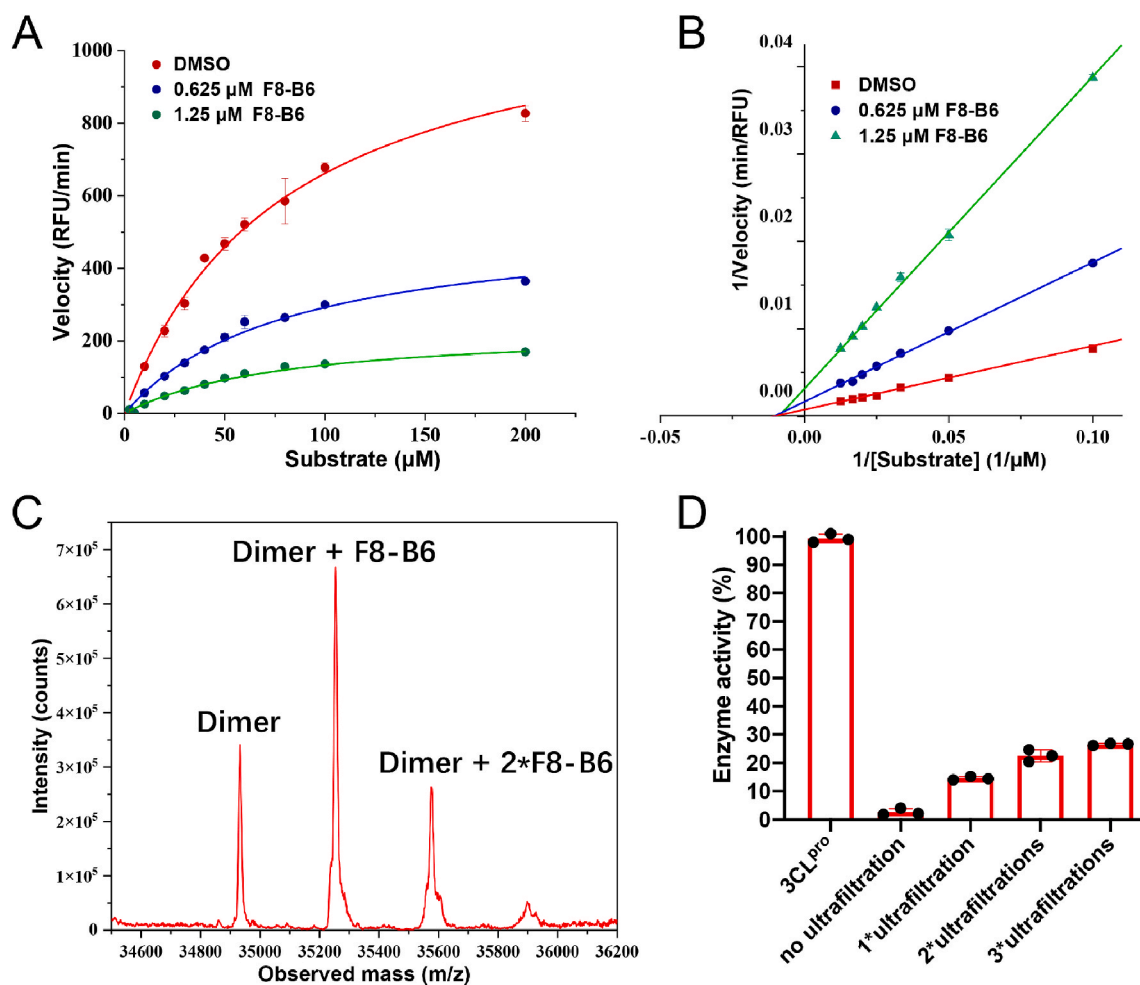
Fig. 4. Michaelis-Menten kinetics analysis (A) and Lineweaver-Burk plot (B) of SARS-CoV-2 M^{pro} in presence or absence of **F8–B6**. (C) The liquid chromatograph-mass spectrometer of SARS-CoV-2 M^{pro} with **F8–B6**. (D) Reversibility assay of the inhibition ability of **F8–B6** against SARS-CoV-2 M^{pro}.
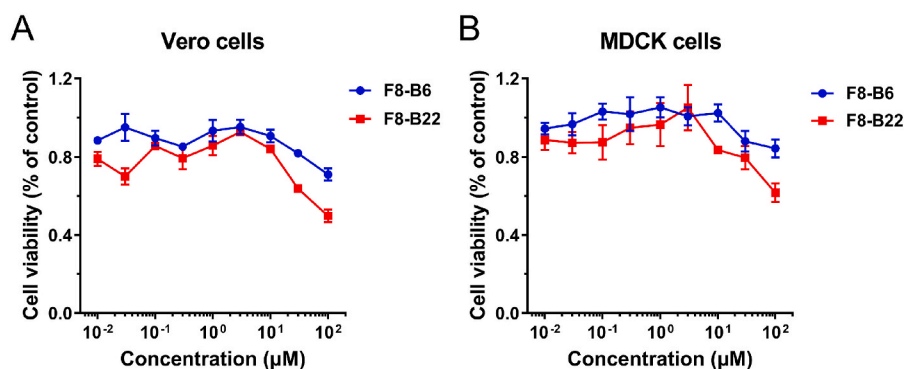
Fig. 5. The cytotoxicity of compounds **F8–B6** and **F8–B22** in Vero (A) and MDCK cells (B).

mmol), corresponding boronic acid (1.2 mmol), tetrakis(triphenyl-phosphine)palladium (0.05 mmol), and potassium carbonate (3 mmol). The vessel was evacuated and backfilled with argon. A mixed solvent of Toluene/EtOH/H$_2$O (5/5/2 mL) was added. Then the schlenk tube was heated to 90 °C overnight. After cooling to room temperature, the reaction mixture was concentrated and diluted with water, filtered and the filtrate was adjusted to pH 2 with 2 N HCl. The precipitate was filtered and dried *in vacuo* to give the crude products without further purification.

4.1.2. General procedure B

A schlenk tube was charged with (5-formylfuran-2-yl)boronic acid (1.5 mmol), substituted bromobenzene (1 mmol), Pd(PPh$_3$)$_2$Cl$_2$ (0.05 mmol), and sodium carbonate (2 mmol). The vessel was evacuated and backfilled with argon. A mixed solvent of MeCN/H$_2$O (4/1.3 mL) was added. Then the schlenk tube was heated to 60 °C overnight. After cooling to room temperature, the reaction mixture was concentrated and diluted with water, filtered and the filtrate was adjusted to pH 2 with 2 N HCl. The precipitate was filtered and dried *in vacuo* to give the crude products without further purification.

4.1.3. General procedure C

A mixture of (5-formylfuran-2-yl)boronic acid (1.5 mmol), substituted bromobenzene (1 mmol), Pd(PPh$_3$)$_2$Cl$_2$ (0.05 mmol) in DME/EtOH (3/3 mL), and 2 M aqueous Na$_2$CO$_3$ (3 mL, 6 mmol of Na$_2$CO$_3$) was flushed with nitrogen for 3 min and heated at 60 °C overnight under nitrogen atmosphere. The solvents were removed under reduced pressure, the residue was dissolved in water, the mixture obtained was filtered through Celite, and the filtrate was adjusted to pH 2 with 2 N HCl. The precipitate was filtered and dried *in vacuo* to give the crude products without further purification.

4.1.4. General procedure D

To a solution of the corresponding aldehyde (1.0 mmol) in MeOH (5.0 mL) was added thiosemicarbazide or substituted thiosemicarbazide (1.05 mmol). The mixture was heated to 50 °C and stirred for 4 h. The residue was recrystallized from ethanol, and the precipitate was filtered and dried *in vacuo* to give target compounds.

4.1.5. (E)-N-(1,5-dimethyl-3-oxo-2-phenyl-2,3-dihydro-1H-pyrazol-4-yl)-2-((5-(4-nitrophenyl)furan-2-yl)methylene)hydrazine-1-carbothioamide (F8–S43)

Compound **F8–S43** was purchased from commercial database. Reddish brown solid. ^{1}H NMR (400 MHz, DMSO-*d*$_6$) δ 12.05 (s, 1H), 9.21 (s, 1H), 8.27 (d, *J* = 8.9 Hz, 2H), 8.09 (s, 2H), 8.07 (s, 1H), 7.52 (t, *J* = 7.8 Hz, 2H), 7.47 (d, *J* = 3.6 Hz, 1H), 7.38 (dt, *J* = 8.4, 1.1 Hz, 2H), 7.36–7.30 (m, 1H), 7.24 (d, *J* = 3.7 Hz, 1H), 3.12 (s, 3H), 2.19 (s, 3H). ^{13}C NMR (100 MHz, DMSO-*d*$_6$) δ 178.70, 162.73, 154.95, 152.84, 151.43, 146.73, 135.70, 135.67, 132.34, 129.57, 126.67, 125.12, 124.85, 123.94, 116.30, 113.06, 109.85, 36.36, 11.66. HRMS (ESI) [M + H] + calcd for C$_{23}$H$_{21}$N$_6$O$_4$S: 477.1345; found: 477.1341.

4.1.6. (E)-3-(5-((2-carbamothioylhydrazono)methyl)furan-2-yl)benzoic acid (F8-A1)

Following the general procedures A and D, compound **F8-A1** was obtained in 42% yield. Yellowish solid. ^{1}H NMR (400 MHz, DMSO-*d*$_6$) δ 13.18 (s, 1H), 11.53 (s, 1H), 8.29 (s, 2H), 8.07 (d, *J* = 7.6 Hz, 1H), 8.00 (s, 1H), 7.89 (d, *J* = 7.6 Hz, 1H), 7.79 (s, 1H), 7.57 (t, *J* = 7.6 Hz, 1H), 7.24 (d, *J* = 3.6 Hz, 1H), 7.11 (d, *J* = 3.6 Hz, 1H). ^{13}C NMR (100 MHz, DMSO-*d*$_6$) δ 178.18, 167.43, 153.97, 149.98, 132.40, 132.11, 130.33, 129.84, 129.22, 128.54, 124.82, 115.54, 109.70. HRMS (ESI) [M − H]⁻ calcd for C$_{13}$H$_{10}$N$_3$O$_3$S⁻: 288.0448; found: 288.0442.

4.1.7. (E)-4-(5-((2-carbamothioylhydrazono)methyl)furan-2-yl)benzoic acid (F8-A2)

Following the general procedures A and D, compound **F8-A2** was obtained in 59% yield. Yellowish solid. ^{1}H NMR (400 MHz, DMSO-*d*$_6$) δ 13.00 (s, 1H), 11.56 (s, 1H), 8.33 (s, 1H), 8.02–7.90 (m, 5H), 7.83 (s, 1H), 7.27 (d, *J* = 3.6 Hz, 1H), 7.10 (d, *J* = 3.6 Hz, 1H). ^{13}C NMR (100 MHz, DMSO-*d*$_6$) δ 178.25, 167.35, 153.85, 150.44, 133.67, 132.14, 130.44, 130.22, 124.29, 115.78, 110.93. HRMS (ESI) [M − H]⁻ calcd for C$_{13}$H$_{10}$N$_3$O$_3$S⁻: 288.0448; found: 288.0442.

4.1.8. (E)-3-(5-((2-(methylcarbamothioyl)hydrazono)methyl)furan-2-yl)benzoic acid (F8-A3)

Following the general procedures A and D, compound **F8-A3** was obtained in 62% yield. Yellowish solid. ^{1}H NMR (400 MHz, DMSO-*d*$_6$) δ 13.19 (s, 1H), 11.56 (s, 1H), 8.40–8.32 (m, 1H), 8.30 (s, 1H), 8.07 (d, *J* = 7.6 Hz, 1H), 8.01 (s, 1H), 7.89 (d, *J* = 7.6 Hz, 1H), 7.59 (t, *J* = 7.8 Hz, 1H), 7.25 (d, *J* = 3.6 Hz, 1H), 7.08 (d, *J* = 3.6 Hz, 1H), 3.03 (d, *J* = 4.4 Hz, 3H). ^{13}C NMR (100 MHz, DMSO-*d*$_6$) δ 177.93, 167.42, 153.94, 150.10, 132.08, 132.05, 130.35, 129.83, 129.22, 128.54, 124.84, 115.41, 109.77, 31.37. HRMS (ESI) [M − H]⁻ calcd for C$_{14}$H$_{12}$N$_3$O$_3$S⁻: 302.0605; found: 302.0601.

4.1.9. (E)-4-(5-((2-(methylcarbamothioyl)hydrazono)methyl)furan-2-yl)benzoic acid (F8-A4)

Following the general procedure, compound **F8-A4** was obtained in 51% yield. Yellowish solid. ^{1}H NMR (400 MHz, DMSO-*d*$_6$) δ 13.01 (s, 1H), 11.61 (s, 1H), 8.34 (q, *J* = 4.6 Hz, 1H), 8.03–7.90 (m, 5H), 7.28 (d, *J* = 3.6 Hz, 1H), 7.09 (d, *J* = 3.6 Hz, 1H), 3.05 (d, *J* = 4.4 Hz, 3H). ^{13}C NMR (100 MHz, DMSO-*d*$_6$) δ 177.97, 167.33, 153.79, 150.56, 133.66, 131.75, 130.43, 130.22, 124.24, 115.54, 110.97, 31.37. HRMS (ESI) [M − H]⁻ calcd for C$_{14}$H$_{12}$N$_3$O$_3$S⁻: 302.0605; found: 302.0600.

4.1.10. (E)-3-(5-((2-((4-chlorophenyl)carbamothioyl)hydrazono)methyl)furan-2-yl)benzoic acid (F8-A5)

Following the general procedures A and D, compound **F8-A5** was obtained in 74% yield. Yellowish solid. ^{1}H NMR (400 MHz, DMSO-*d*$_6$) δ 12.97 (s, 1H), 12.01 (s, 1H), 10.05 (s, 1H), 8.33 (s, 1H), 8.12 (s, 1H), 8.08 (d, *J* = 7.8 Hz, 1H), 7.90 (d, *J* = 7.8 Hz, 1H), 7.65 (d, *J* = 8.4 Hz, 2H), 7.59 (t, *J* = 7.6 Hz, 1H), 7.43 (d, *J* = 8.4 Hz, 2H), 7.28 (d, *J* = 3.6 Hz, 1H), 7.24 (d, *J* = 3.6 Hz, 1H). ^{13}C NMR (100 MHz, DMSO-*d*$_6$) δ 176.09, 167.40, 154.29, 149.87, 138.48, 133.14, 132.09, 130.28, 129.87, 129.72, 129.31, 128.61, 128.49, 127.54, 124.91, 116.16, 109.87. HRMS (ESI) [M − H]⁻ calcd for C$_{19}$H$_{13}$ClN$_3$O$_3$S⁻: 398.0372; found: 398.0366.

4.1.11. (E)-4-(5-((2-((4-chlorophenyl)carbamothioyl)hydrazono)methyl)furan-2-yl)benzoic acid (F8-A6)

Following the general procedures A and D, compound **F8-A6** was obtained in 51% yield. Yellowish solid. ^{1}H NMR (400 MHz, DMSO-*d*$_6$) δ 13.02 (s, 1H), 12.03 (s, 1H), 10.03 (s, 1H), 8.12 (s, 1H), 8.00 (d, *J* = 8.4 Hz, 2H), 7.95 (d, *J* = 8.4 Hz, 2H), 7.64 (d, *J* = 8.8 Hz, 2H), 7.43 (d, *J* = 8.8 Hz, 2H), 7.33 (d, *J* = 3.6 Hz, 1H), 7.25 (d, *J* = 3.6 Hz, 1H). ^{13}C NMR (100 MHz, DMSO-*d*$_6$) δ 176.22, 167.32, 154.19, 150.36, 138.47, 133.60, 132.95, 130.47, 130.32, 129.86, 128.49, 127.86, 124.35, 116.32, 111.12. HRMS (ESI) [M − H]⁻ calcd for C$_{19}$H$_{13}$ClN$_3$O$_3$S⁻: 398.0372; found: 398.0361.

4.1.12. (E)-3-(5-((2-((3-(trifluoromethyl)phenyl)carbamothioyl)hydrazono)methyl)furan-2-yl)benzoic acid (F8-A7)

Following the general procedures A and D, compound **F8-A7** was obtained in 35% yield. Yellowish solid. ^{1}H NMR (400 MHz, DMSO-*d*$_6$) δ 12.11 (s, 1H), 10.23 (s, 1H), 8.33 (s, 1H), 8.15 (s, 1H), 8.12–8.03 (m, 2H), 7.98–7.87 (m, 2H), 7.65–7.53 (m, 3H), 7.31–7.21 (m, 2H). ^{13}C NMR (100 MHz, DMSO-*d*$_6$) δ 176.15, 167.40, 154.41, 149.86, 140.33, 133.51, 132.12, 130.26, 129.84, 129.71, 129.64, 129.33, 129.29 (d, *J* = 31.9 Hz), 128.60, 124.95, 124.54 (q, *J* = 273.3 Hz), 122.11 (d, *J* = 4.0 Hz), 122.03, 116.24, 109.87. ^{19}F NMR (376 MHz, DMSO-*d*$_6$) δ −61.11. HRMS (ESI) [M − H]⁻ calcd for C$_{20}$H$_{13}$F$_3$N$_3$O$_3$S⁻: 432.0635; found: 432.0623.

4.1.13. (E)-4-(5-((2-((3-(trifluoromethyl)phenyl)carbamothioyl)hydrazono)methyl)furan-2-yl)benzoic acid (F8-A8)

Following the general procedures A and D, compound **F8-A8** was obtained in 51% yield. Yellowish solid. ^{1}H NMR (400 MHz, DMSO-*d*$_6$) δ 13.01 (s, 1H), 12.13 (s, 1H), 10.20 (s, 1H), 8.18–7.89 (m, 7H), 7.68–7.52 (m, 2H), 7.34 (d, *J* = 3.6 Hz, 1H), 7.27 (d, *J* = 3.6 Hz, 1H). ^{13}C NMR (100 MHz, DMSO-*d*$_6$) δ 176.21, 167.35, 154.31, 150.32, 140.26, 133.54, 133.29, 130.44, 130.37, 129.79, 129.56, 129.21, 124.50 (q, *J* = 273.4 Hz), 124.29, 122.27 (d, *J* = 4.0 Hz), 122.04, 116.31, 110.98. ^{19}F NMR (376 MHz, DMSO-*d*$_6$) δ −61.15. HRMS (ESI) [M − H]⁻ calcd for C$_{20}$H$_{13}$F$_3$N$_3$O$_3$S⁻: 432.0635; found: 432.0627.

4.1.14. (E)-4-(5-((2-(cyclohexylcarbamothioyl)hydrazono)methyl)furan-2-yl)benzoic acid (F8-A9)

Following the general procedures A and D, compound **F8-A9** was obtained in 74% yield. Yellowish solid. ^{1}H NMR (400 MHz, DMSO-*d*$_6$) δ 13.01 (s, 1H), 11.58 (s, 1H), 8.13–7.78 (m, 6H), 7.30 (d, *J* = 3.6 Hz, 1H), 7.16 (d, *J* = 3.6 Hz, 1H), 4.28–4.08 (m, 1H), 2.01–1.05 (m, 10H). [13]C

NMR (100 MHz, DMSO-d_6) δ 175.93, 167.30, 153.89, 150.50, 133.61, 132.04, 130.48, 130.24, 124.22, 115.65, 111.06, 52.97, 32.24, 25.54, 25.24. HRMS (ESI) [M − H]⁻ calcd for $C_{19}H_{20}N_3O_3S^-$: 370.1231; found: 370.1225.

4.1.15. (E)-4-(5-((2-carbamothioylhydrazono)methyl)furan-2-yl) benzamide (F8–B1)

Following the general procedures B and D, compound **F8–B1** was obtained in 44% yield. Yellowish solid. ¹H NMR (400 MHz, DMSO-d_6) δ 11.54 (s, 1H), 8.31 (s, 1H), 8.05 (s, 1H), 8.02–7.81 (m, 6H), 7.43 (s, 1H), 7.24 (d, J = 3.6 Hz, 1H), 7.09 (d, J = 3.6 Hz, 1H). ¹³C NMR (100 MHz, DMSO-d_6) δ 178.18, 167.78, 154.16, 150.10, 133.78, 132.32, 132.22, 128.65, 124.08, 115.86, 110.30. HRMS (ESI) [M − H]⁻ calcd for $C_{13}H_{11}N_4O_2S^-$: 287.0608; found: 287.0604.

4.1.16. (E)-2-((5-(4-sulfamoylphenyl)furan-2-yl)methylene)hydrazine-1-carbothioamide (F8–B2)

Following the general procedures B and D, compound **F8–B2** was obtained in 63% yield. Yellowish solid. ¹H NMR (400 MHz, DMSO-d_6) δ 11.57 (s, 1H), 8.34 (s, 1H), 8.09–7.76 (m, 6H), 7.42 (s, 2H), 7.28 (d, J = 3.6 Hz, 1H), 7.11 (d, J = 3.6 Hz, 1H). ¹³C NMR (100 MHz, DMSO-d_6) δ 178.23, 153.41, 150.46, 143.45, 132.77, 132.04, 126.82, 124.59, 115.77, 110.99. HRMS (ESI) [M − H]⁻ calcd for $C_{12}H_{11}N_4O_3S_2^-$: 323.0278; found: 323.0275.

4.1.17. (E)-2-((5-phenylfuran-2-yl)methylene)hydrazine-1-carbothioamide (F8–B3) [44,45]

Following the general procedures C and D, compound **F8–B3** was obtained in 24% yield. Yellowish solid. ¹H NMR (400 MHz, DMSO-d_6) δ 11.50 (s, 1H), 8.33–8.25 (m, 1H), 7.97 (s, 1H), 7.87–7.81 (m, 2H) 7.78 (s, 1H), 7.47–7.41 (m, 2H), 7.38–7.30 (m, 1H), 7.12 (d, J = 3.6 Hz, 1H), 7.07 (d, J = 3.6 Hz, 1H).

4.1.18. (E)-4-(5-((2-carbamothioylhydrazono)methyl)furan-2-yl)-3-fluorobenzoic acid (F8–B4)

Following the general procedures A and D, compound **F8–B4** was obtained in 51% yield. Orange red solid. ¹H NMR (400 MHz, DMSO-d_6) δ 13.33 (s, 1H), 11.60 (s, 1H), 8.36 (s, 1H), 8.11 (t, J = 8.0 Hz, 1H), 8.01 (s, 1H), 7.93–7.71 (m, 3H), 7.20–7.09 (m, 3H). ¹³C NMR (100 MHz, DMSO-d_6) δ 178.35, 166.32 (d, J = 2.5 Hz), 158.00 (d, J = 252.1 Hz), 150.58, 147.97 (d, J = 3.4 Hz), 131.95 (d, J = 7.8 Hz), 131.79, 126.75 (d, J = 1.9 Hz), 126.26 (d, J = 3.1 Hz), 121.76 (d, J = 11.9 Hz), 117.16 (d, J = 22.5 Hz), 115.59, 114.91 (d, J = 12.3 Hz). ¹⁹F NMR (376 MHz, DMSO-d_6) δ −113.32. HRMS (ESI) [M − H]⁻ calcd for $C_{13}H_9FN_3O_3S^-$: 306.0354; found: 306.0347.

4.1.19. (E)-4-(5-((2-carbamothioylhydrazono)methyl)furan-2-yl)-3-methylbenzoic acid (F8–B5)

Following the general procedures B and D, compound **F8–B5** was obtained in 56% yield. Yellowish solid. ¹H NMR (400 MHz, DMSO-d_6) δ 12.97 (s, 1H), 11.56 (s, 1H), 8.32 (s, 1H), 8.01 (s, 1H), 7.95 (d, J = 8.2 Hz, 1H), 7.89–7.75 (m, 3H), 7.14 (d, J = 3.6 Hz, 1H), 7.04 (d, J = 3.6 Hz, 1H), 2.53 (s, 3H). ¹³C NMR (100 MHz, DMSO-d_6) δ 178.23, 167.43, 153.33, 149.90, 134.80, 132.91, 132.76, 132.26, 130.00, 127.58, 127.07, 115.43, 113.80, 22.29. HRMS (ESI) [M − H]⁻ calcd for $C_{14}H_{12}N_3O_3S^-$: 302.0605; found: 302.0597.

4.1.20. (E)-4-(5-((2-carbamothioylhydrazono)methyl)furan-2-yl)-2-hydroxybenzoic acid (F8–B6)

Following the general procedures A and D, compound **F8–B6** was obtained in 73% yield. Yellowish solid. ¹H NMR (400 MHz, DMSO-d_6) δ 11.56 (s, 1H), 8.31 (s, 1H), 7.98 (s, 1H), 7.87 (s, 1H), 7.81 (d, J = 8.0 Hz, 1H), 7.45–7.34 (m, 2H), 7.28 (d, J = 3.6 Hz, 1H), 7.09 (d, J = 3.6 Hz, 1H). ¹³C NMR (100 MHz, DMSO-d_6) δ 178.22, 172.05, 161.99, 153.45, 150.60, 136.16, 132.09, 131.42, 115.75, 115.32, 112.49, 112.02, 111.65. HRMS (ESI) [M − H]⁻ calcd for $C_{13}H_{10}N_3O_4S^-$: 304.0398; found:

304.0394.

4.1.21. (E)-4-(5-((2-carbamothioylhydrazono)methyl)furan-2-yl)-2-chlorobenzoic acid (F8–B7)

Following the general procedures A and D, compound **F8–B7** was obtained in 83% yield. Yellowish solid. ¹H NMR (400 MHz, DMSO-d_6) δ 13.36 (s, 1H), 11.57 (s, 1H), 8.31 (s, 1H), 8.06–7.77 (m, 5H), 7.31 (d, J = 3.6 Hz, 1H), 7.08 (d, J = 3.6 Hz, 1H). ¹³C NMR (100 MHz, DMSO-d_6) δ 178.27, 166.61, 152.36, 150.78, 133.68, 133.44, 132.32, 132.05, 129.98, 125.85, 122.65, 115.79, 111.76. HRMS (ESI) [M − H]⁻ calcd for $C_{13}H_9ClN_3O_5S^-$: 322.0059; found: 32.0053.

4.1.22. (E)-3-(5-((2-carbamothioylhydrazono)methyl)furan-2-yl)-2-chlorobenzoic acid (F8–B8)

Following the general procedures C and D, compound **F8–B8** was obtained in 53% yield. Yellowish solid. ¹H NMR (400 MHz, DMSO-d_6) δ 13.54 (br, 1H), 11.56 (s, 1H), 8.32 (s, 1H), 8.12 (d, J = 8.0 Hz, 1H), 8.00 (s, 1H), 7.82 (s, 1H), 7.63 (dd, J = 8.0, 1.8 Hz, 1H), 7.52 (t, J = 7.6 Hz, 1H), 7.33 (d, J = 3.6 Hz, 1H), 7.14 (d, J = 3.6 Hz, 1H). ¹³C NMR (100 MHz, DMSO-d_6) δ 178.30, 167.77, 150.56, 149.94, 135.47, 132.05, 130.65, 129.45, 129.26, 127.96, 127.01, 115.12, 114.65. HRMS (ESI) [M − H]⁻ calcd for $C_{13}H_9ClN_3O_3S^-$: 322.0059; found: 322.0059.

4.1.23. (E)-5-(5-((2-carbamothioylhydrazono)methyl)furan-2-yl)-2-chlorobenzoic acid (F8–B9)

Following the general procedures A and D, compound **F8–B9** was obtained in 50% yield. Yellowish solid. ¹H NMR (400 MHz, DMSO-d_6) δ 13.61 (s, 1H), 11.54 (s, 1H), 8.30 (s, 1H), 8.13 (s, 1H), 8.03–7.91 (m, 2H), 7.83 (s, 1H), 7.60 (d, J = 8.4 Hz, 1H), 7.27 (d, J = 3.6 Hz, 1H), 7.09 (d, J = 3.6 Hz, 1H). ¹³C NMR (100 MHz, DMSO-d_6) δ 178.22, 166.96, 152.92, 150.19, 132.98, 132.15, 131.65, 130.95, 128.96, 127.81, 125.91, 115.72, 110.31. HRMS (ESI) [M − H]⁻ calcd for $C_{13}H_9ClN_3O_3S^-$: 322.0059; found: 322.0059.

4.1.24. (E)-3-(5-((2-carbamothioylhydrazono)methyl)furan-2-yl)-4-chlorobenzoic acid (F8–B10)

Following the general procedures C and D, compound **F8–B10** was obtained in 73% yield. Yellowish solid. ¹H NMR (400 MHz, DMSO-d_6) δ 13.34 (s, 1H), 11.60 (s, 1H), 8.38 (d, J = 2.1 Hz, 1H), 8.33 (s, 1H), 8.04 (s, 1H), 7.85 (dd, J = 8.4, 2.1 Hz, 1H), 7.78 (s, 1H), 7.68 (d, J = 8.4 Hz, 1H), 7.34 (d, J = 3.6 Hz, 1H), 7.20 (d, J = 3.6 Hz, 1H). ¹³C NMR (100 MHz, DMSO-d_6) δ 178.32, 166.64, 150.43, 150.05, 133.93, 132.30, 131.82, 130.68, 129.98, 129.03, 128.37, 114.58, 114.26. HRMS (ESI) [M − H]⁻ calcd for $C_{13}H_9N_3O_3S^-$: 322.0059; found: 322.0057.

4.1.25. (E)-3-(5-((2-carbamothioylhydrazono)methyl)furan-2-yl)-2-methoxybenzoic acid (F8–B11)

Following the general procedures C and D, compound **F8–B11** was obtained in 59% yield. Yellowish solid. ¹H NMR (400 MHz, DMSO-d_6) δ 13.14 (s, 1H), 11.54 (s, 1H), 8.31 (s, 1H), 8.12 (d, J = 7.6 Hz, 1H), 8.00 (s, 1H), 7.81 (s, 1H), 7.66 (d, J = 7.6 Hz, 1H), 7.29 (t, J = 7.6 Hz, 1H), 7.11 (s, 2H), 3.79 (s, 3H). ¹³C NMR (100 MHz, DMSO-d_6) δ 178.17, 167.60, 155.87, 150.57, 149.05, 132.21, 130.84, 130.10, 127.46, 124.60, 124.41, 116.02, 113.14, 61.64. HRMS (ESI) [M − H]⁻ calcd for $C_{14}H_{12}N_3O_4S^-$: 318.0554; found: 318.0549.

4.1.26. (E)-5-(5-((2-carbamothioylhydrazono)methyl)furan-2-yl)-2-hydroxybenzoic acid (F8–B12)

Following the general procedures A and D, compound **F8–B12** was obtained in 67% yield. Yellowish solid. ¹H NMR (400 MHz, DMSO-d_6) δ 11.48 (s, 1H), 8.25 (s, 1H), 8.14 (d, J = 2.4 Hz, 1H), 8.00–7.92 (m, 2H), 7.74 (s, 1H), 7.07–6.98 (m, 3H). ¹³C NMR (100 MHz, DMSO-d_6) δ 178.04, 171.94, 161.37, 154.31, 149.03, 132.64, 131.79, 125.98, 121.69, 118.40, 115.84, 113.94, 107.60. HRMS (ESI) [M − H]⁻ calcd for $C_{13}H_{10}N_3O_4S^-$: 304.0398; found: 304.0394.

4.1.27. (E)-2-((5-(3-cyano-4-hydroxyphenyl)furan-2-yl)methylene) hydrazine-1-carbothioamide (F8–B13)

Following the general procedures A and D, compound **F8–B13** was obtained in 52% yield. Pale brown solid. ^{1}H NMR (400 MHz, DMSO-d_6) δ 11.49 (s, 1H), 11.43 (s, 1H), 8.27 (s, 1H), 8.10 (d, $J = 2.4$ Hz, 1H), 7.99–7.90 (m, 2H), 7.81 (s, 1H), 7.13–6.97 (m, 3H). ^{13}C NMR (100 MHz, DMSO-d_6) δ 178.07, 160.43, 153.52, 149.07, 132.16, 130.84, 129.19, 122.12, 117.25, 116.99, 116.13, 107.94, 100.05. HRMS (ESI) [M − H]$^-$ calcd for $C_{13}H_9N_4O_2S^-$: 285.0452; found: 285.0448.

4.1.28. (E)-2-((5-(3,4-dimethoxyphenyl)furan-2-yl)methylene)hydrazine-1-carbothioamide (F8–B14)

Following the general procedures A and D, compound **F8–B14** was obtained in 71% yield. Yellowish solid. ^{1}H NMR (400 MHz, DMSO-d_6) δ 11.47 (s, 1H), 8.24 (s, 1H), 7.97 (s, 1H), 7.75 (s, 1H), 7.38 (d, $J = 9.2$ Hz, 1H), 7.34 (s, 1H), 7.08–6.97 (m, 3H), 3.84 (s, 3H), 3.79 (s, 3H). ^{13}C NMR (100 MHz, DMSO-d_6) δ 178.01, 155.40, 149.62, 149.52, 148.77, 132.57, 122.98, 117.44, 115.97, 112.47, 108.26, 107.47, 56.17, 56.02. HRMS (ESI) [M + H]$^+$ calcd for $C_{14}H_{16}N_3O_3S^+$: 306.0907; found: 306.0906.

4.1.29. (E)-2-((5-(3,4-dichlorophenyl)furan-2-yl)methylene) hydrazine-1-carbothioamide (F8–B15)

Following the general procedures A and D, compound **F8–B15** was obtained in 63% yield. Yellowish solid. ^{1}H NMR (400 MHz, DMSO-d_6) δ 11.55 (s, 1H), 8.31 (s, 1H), 8.08 (s, 1H), 7.96 (s, 1H), 7.87 (s, 1H), 7.81 (d, $J = 8.4$ Hz, 1H), 7.68 (d, $J = 8.4$ Hz, 1H), 7.28 (d, $J = 3.6$ Hz, 1H), 7.08 (d, $J = 3.6$ Hz, 1H). ^{13}C NMR (100 MHz, DMSO-d_6) δ 178.25, 152.37, 150.29, 132.40, 131.94, 131.60, 130.71, 130.50, 125.90, 124.44, 115.86, 110.73. HRMS (ESI) [M − H]$^-$ calcd for $C_{12}H_8Cl_2N_3OS^-$: 311.9771; found: 311.9767.

4.1.30. (E)-2-((5-(pyridin-4-yl)furan-2-yl)methylene)hydrazine-1-carbothioamide (F8–B16)

Following the general procedures A and D, compound **F8–B16** was obtained in 72% yield. Yellowish solid. ^{1}H NMR (400 MHz, DMSO-d_6) δ 11.60 (s, 1H), 8.60 (d, $J = 5.2$ Hz, 2H), 8.36 (s, 1H), 7.99 (s, 1H), 7.87 (s, 1H), 7.76 (d, $J = 5.2$ Hz, 2H), 7.41 (d, $J = 3.6$ Hz, 1H), 7.19 (d, $J = 3.6$ Hz, 1H) ^{13}C NMR (100 MHz, DMSO-d_6) δ 178.36, 152.14, 151.11, 150.72, 136.44, 131.84, 118.24, 115.41, 112.49. HRMS (ESI) [M − H]$^-$ calcd for $C_{11}H_9N_4OS^-$: 245.0497; found: 245.0502.

4.1.31. (E)-2-((5-(6-fluoropyridin-3-yl)furan-2-yl)methylene)hydrazine-1-carbothioamide (F8–B17)

Following the general procedures A and D, compound **F8–B17** was obtained in 61% yield. Yellowish solid. ^{1}H NMR (400 MHz, DMSO-d_6) δ 11.54 (s, 1H), 8.73 (d, $J = 2.4$ Hz, 1H), 8.42–8.27 (m, 2H), 7.97 (s, 1H), 7.92–7.80 (m, 1H), 7.26 (dd, $J = 8.8, 2.4$ Hz, 1H), 7.20 (d, $J = 3.6$ Hz, 1H), 7.06 (d, $J = 3.6$ Hz, 1H). ^{13}C NMR (100 MHz, DMSO-d_6) δ 178.24, 162.76 (d, $J = 234.7$ Hz), 151.26, 150.12, 143.68 (d, $J = 15.5$ Hz), 137.89 (d, $J = 7.9$ Hz), 131.90, 124.85 (d, $J = 4.4$ Hz), 115.68, 110.45 (d, $J = 37.9$ Hz), 109.96. ^{19}F NMR (376 MHz, DMSO-d_6) δ −69.11. HRMS (ESI) [M − H]$^-$ calcd for $C_{11}H_8FN_4OS^-$: 263.0408; found: 263.0403.

4.1.32. (E)-2-((5-(naphthalen-1-yl)furan-2-yl)methylene)hydrazine-1-carbothioamide (F8–B18)

Following the general procedures A and D, compound **F8–B18** was obtained in 79% yield. Yellowish solid. ^{1}H NMR (400 MHz, DMSO-d_6) δ 11.56 (s, 1H), 8.40 (d, $J = 8.0$ Hz, 1H), 8.30 (s, 1H), 8.08 (s, 1H), 8.02–7.99 (m, 2H), 7.89 (dd, $J = 7.2, 1.2$ Hz, 1H), 7.74 (s, 1H), 7.64–7.56 (m, 3H), 7.21 (d, $J = 3.2$ Hz, 1H), 7.11 (d, $J = 3.2$ Hz, 1H) ^{13}C NMR (100 MHz, DMSO-d_6) δ 178.20, 154.42, 149.96, 134.04, 132.70, 129.70, 129.64, 129.19, 127.73, 127.34, 126.87, 126.72, 125.99, 125.30, 115.12, 112.67. HRMS (ESI) [M − H]$^-$ calcd for $C_{16}H_{13}N_3OS^-$: 294.0701; found: 294.0703.

4.1.33. (E)-2-((5-(naphthalen-2-yl)furan-2-yl)methylene)hydrazine-1-carbothioamide (F8–B19)

Following the general procedures A and D, compound **F8–B19** was obtained in 45% yield. Yellowish solid. ^{1}H NMR (400 MHz, DMSO-d_6) δ 11.57 (s, 1H), 8.37 (s, 1H), 8.34 (s, 1H), 8.06–7.79 (m, 6H), 7.60–7.48 (m, 2H), 7.25 (d, $J = 3.6$ Hz, 1H), 7.13 (d, $J = 3.6$ Hz, 1H). ^{13}C NMR (100 MHz, DMSO-d_6) δ 178.16, 155.05, 149.79, 133.53, 133.00, 132.38, 129.03, 128.59, 128.19, 127.38, 127.29, 126.91, 122.77, 115.91, 109.55. HRMS (ESI) [M − H]$^-$ calcd for $C_{16}H_{12}N_3OS^-$: 294.0707; found: 294.0705.

4.1.34. (E)-2-((5-(quinolin-7-yl)furan-2-yl)methylene)hydrazine-1-carbothioamide (F8–B20)

Following the general procedures A and D, compound **F8–B20** was obtained in 56% yield. Yellowish solid. ^{1}H NMR (400 MHz, DMSO-d_6) δ 11.62 (s, 1H), 8.86 (dd, $J = 4.0, 2.0$ Hz, 1H), 8.47–8.34 (m, 3H), 8.17 (dd, $J = 8.8, 2.0$ Hz, 1H), 8.03 (d, $J = 9.8$ Hz, 2H), 7.92–7.83 (m, 1H), 7.53 (dd, $J = 8.4, 4.0$ Hz, 1H), 7.28 (d, $J = 3.6$ Hz, 1H), 7.13 (d, $J = 3.6$ Hz, 1H). ^{13}C NMR (100 MHz, DMSO-d_6) δ 178.21, 154.33, 151.12, 150.16, 147.77, 136.61, 132.29, 130.11, 128.60, 127.82, 126.33, 122.75, 122.66, 115.83, 110.22. HRMS (ESI) [M − H]$^-$ calcd for $C_{15}H_{11}N_4OS^-$: 295.0659; found: 295.0654.

4.1.35. (E)-2-((5-(quinolin-3-yl)furan-2-yl)methylene)hydrazine-1-carbothioamide (F8–B21)

Following the general procedures A and D, compound **F8–B21** was obtained in 71% yield. Yellowish solid. ^{1}H NMR (400 MHz, DMSO-d_6) δ 11.60 (s, 1H), 9.39 (s, 1H), 8.72 (s, 1H), 8.37 (s, 1H), 8.11–7.97 (m, 3H), 7.89 (s, 1H), 7.75 (t, $J = 7.6$ Hz, 1H), 7.64 (t, $J = 7.6$ Hz, 1H), 7.42 (d, $J = 3.6$ Hz, 1H), 7.17 (d, $J = 3.6$ Hz, 1H). ^{13}C NMR (100 MHz, DMSO-d_6) δ 178.25, 152.57, 150.48, 147.60, 147.20, 132.02, 130.20, 129.70, 129.33, 128.81, 127.92, 127.90, 123.38, 115.74, 110.60. HRMS (ESI) [M − H]$^-$ calcd for $C_{15}H_{11}N_4OS^-$: 295.0659; found: 295.0654.

4.1.36. (E)-2-((5-benzylfuran-2-yl)methylene)hydrazine-1-carbothioamide (F8–B22)

5-hydroxymethyl-2-furfuraldehyde (0.31 g, 2.45 mmol) was added to the mixture of TfOH (4 mL) and benzene (0.28 mL) in an ice bath. The reaction mixture was stirred at room temperature for 2 h. The mixture was poured into water (30 mL), and extracted with chloroform (3 × 30 mL). The combined extracts were washed with water, the saturated aqueous solution of NaHCO$_3$, water again, and dried over Na$_2$SO$_4$. The solvent was removed under reduced pressure, and the residue was subjected to chromatographic separation on silica gel to give intermediate 5-(phenylmethyl)furan-2-carbaldehyde 0.1 g, yielding 21%. Then following the general procedure D, compound **F8–B22** was obtained in 42% yield. Yellowish solid. ^{1}H NMR (400 MHz, DMSO-d_6) δ 11.38 (s, 1H), 8.17 (s, 1H), 7.89 (s, 1H), 7.55 (s, 1H), 7.37–7.19 (m, 5H), 6.88 (d, $J = 3.6$ Hz, 1H), 6.26 (d, $J = 3.6$ Hz, 1H), 4.02 (s, 2H). ^{13}C NMR (100 MHz, DMSO-d_6) δ 177.98, 157.32, 148.87, 138.02, 133.07, 129.08, 129.01, 127.03, 114.52, 109.71, 34.18. HRMS (ESI) [M − H]$^-$ calcd for $C_{13}H_{12}N_3OS^-$: 258.0707; found: 258.0699.

4.1.37. (E)-4-(5-((2-carbamothioylhydrazono)methyl)furan-3-yl)benzoic acid (F8–C1)

Following the general procedures A and D, compound **F8–C1** was obtained in 25% yield. Yellowish solid. ^{1}H NMR (400 MHz, DMSO-d_6) δ 12.96 (s, 1H), 11.53 (s, 1H), 8.45 (s, 1H), 8.30 (s, 1H), 8.03–7.92 (m, 3H), 7.81–7.65 (m, 3H), 7.53 (s, 1H). ^{13}C NMR (100 MHz, DMSO-d_6) δ 178.35, 167.45, 151.23, 142.77, 135.97, 132.41, 130.44, 129.88, 127.55, 125.95, 111.02. HRMS (ESI) [M − H]$^-$ calcd for $C_{13}H_{10}N_3O_3S^-$: 288.0448; found: 288.0447.

4.1.38. (E)-4-(5-((2-carbamothioylhydrazono)methyl)thiophen-2-yl) benzoic acid (F8–C2)

Following the general procedures A and D, compound **F8–C2** was

obtained in 51% yield. Yellowish solid. ^1H NMR (400 MHz, DMSO-d_6) δ 13.02 (s, 1H), 11.56 (s, 1H), 8.27 (s, 1H), 8.22 (s, 1H), 7.98 (d, $J = 8.0$ Hz, 2H), 7.81 (d, $J = 8.0$ Hz, 2H), 7.67 (d, $J = 4.0$ Hz, 1H), 7.64 (s, 1H), 7.50 (d, $J = 4.0$ Hz, 1H). ^{13}C NMR (100 MHz, DMSO-d_6) δ 178.09, 167.25, 144.26, 139.89, 137.66, 137.51, 132.33, 130.70, 130.41, 126.43, 125.82. HRMS (ESI) [M − H]$^-$ calcd for $C_{13}H_{10}N_3O_2S^-$: 304.0220; found: 304.0215.

4.1.39. (E)-3'-((2-carbamothioylhydrazono)methyl)-[1,1'-biphenyl]-4-carboxylic acid (F8–C3)

Following the general procedures A and D, compound **F8–C3** was obtained in 23% yield. White solid. ^1H NMR (400 MHz, DMSO-d_6) δ 13.00 (br, 1H), 11.52 (s, 1H), 8.27 (s, 1H), 8.22 (s, 1H), 8.18 (s, 1H), 8.13 (s, 1H), 8.03 (d, $J = 8.0$ Hz, 2H), 7.88 (d, $J = 8.0$ Hz, 2H), 7.79–7.74 (m, 2H), 7.52 (t, $J = 7.4$ Hz, 1H) ^{13}C NMR (100 MHz, DMSO-d_6) δ 178.52, 167.59, 144.13, 142.40, 139.90, 135.50, 130.34, 130.27, 129.88, 128.72, 128.03, 127.48, 125.61. HRMS (ESI) [M − H]$^-$ calcd for $C_{15}H_{13}N_3O_2S^-$: 298.0650; found: 298.0656.

4.1.40. (E)-4'-((2-carbamothioylhydrazono)methyl)-[1,1'-biphenyl]-4-carboxylic acid (F8–C4)

Following the general procedures A and D, compound **F8–C4** was obtained in 12% yield. White solid. ^1H NMR (400 MHz, DMSO-d_6) δ 13.01 (s, 1H), 11.52 (s, 1H), 8.26 (s, 1H), 8.10 (d, $J = 5.1$ Hz, 2H), 8.03 (d, $J = 8.4$ Hz, 2H), 7.92 (d, $J = 8.4$ Hz, 2H), 7.85 (d, $J = 8.4$ Hz, 2H), 7.77 (d, $J = 8.4$ Hz, 2H). ^{13}C NMR (100 MHz, DMSO-d_6) δ 178.47, 167.56, 143.92, 142.08, 140.46, 134.60, 130.45, 130.32, 128.44, 127.62, 127.24. HRMS (ESI) [M − H]$^-$ calcd for $C_{15}H_{13}N_3O_2S^-$: 298.0650; found: 298.0653.

4.2. Reagents and compounds

Tideglusib was purchased from Topscience Co. Ltd. SARS-CoV-2 M^{pro} fluorescent substrate Dabcyl-KTSAVLQSGFRKM-E(Edans)-NH$_2$ was synthesized by GL (Shanghai) Biochem Ltd. (Shanghai, China). Compounds used for SARS-CoV-2 M^{pro} inhibitors screening were purchased from ChemDiv (https://www.chemdiv.com/) and SPECS (https://www.specs.net/) commercial databases.

4.3. Cloning, expression, and purification of SARS-CoV-2 M^{pro}

The full-length gene encoding SARS-CoV-2 M^{pro} was synthesized for *Escherichia coli* (*E. coli*) expression (Hienzyme Biotech). The expression and purification of SARS-CoV-2 M^{pro} were carried out using the reported protocol [29].

4.4. SPR assay

The SPR assay was used to analyze the interaction between SARS-CoV-2 M^{pro} with compounds on a Biacore 8 K instrument (GE Healthcare). SARS-CoV-2 M^{pro} was immobilized on a sensor chip (CM5) via Amine Coupling Kit (GE Healthcare, Buckinghamshire, UK) at levels of approximately 10,000 response units (RU). The first flow channel without immobilized protein was set as a reference, and the compounds were injected at the concentration of 50 μM for screening and 0.2 μM–100 μM for binding study in a period of 60 s. Dissociation was measured for 100–200 s at a flow rate of 30 μL/min using the following assay running buffer: 10 mM phosphate buffer containing 2.7 mM KCl, 137 mM NaCl, and 0.05% surfactant P20 (pH 7.5). All of the data were analyzed through Biacore evaluation software (8 K version 1.0), and the curve was fitted with a 1:1 kinetics binding model.

4.5. Enzymatic assay of SARS-CoV-2 M^{pro}

A fluorescent substrate Dabcyl-KTSAVLQSGFRKM-E(Edans)-NH$_2$ (GL Biochemistry Ltd) and assay buffer (40 mM PBS, 100 mM NaCl, 1 mM EDTA, 0.1% Triton 100, pH 7.3) was used for the inhibition assay. For the preliminary screening and IC$_{50}$ measurements, 0.5 μM protease was incubated with inhibitor at room temperature for 30 min, and then the reaction was initiated by adding 20 μM substrate. The fluorescence signal generated by the cleavage of the substrate was monitored for 20 min at an emission wavelength of 460 nm with excitation at 360 nm using a plate reader (Synergy, Biotek). IC$_{50}$ values were fitted with the Hill1 function of Origin 2018. For the enzymatic kinetic assay, 0.5 μM SARS-CoV-2 M^{pro} was pre-incubated with DMSO or **F8–B6** for 3 h and different concentrations of the fluorescent substrate were added to initiate the reaction. Data was collected from three replicates and curve-fitted by Origin 2018. For the DTT assay, 0.5 μM SARS-CoV-2 M^{pro} was premixed with 400 mM DTT or H$_2$O. Then, the protease solution was co-preincubated with DMSO or inhibitor at various concentrations for 30 min. Enzyme activity was tested and data was collected from three replicates. For time-dependent inhibitory measurement, various concentrations of inhibitors were pre-incubated with SARS-CoV-2 M^{pro} at a different time at room temperature before the addition of fluorescent substrate.

4.6. Mass spectrometry

2 μM protease was co-incubated with 15 μM F8–B6 on ice for 3 h. Then, the complex solution was analyzed by Quadrupole-TOF LC-MS/MS System (Vion, Waters). Raw data of mass signal was deconvoluted to obtain the total mass of the protein.

4.7. Enzymatic reversibility assay

SARS-CoV-2 M^{pro} (10 μM) was incubated with 100 μM **F8–B6** for 180 min and divided into four parts which were ultra-filtrated for different times. In each time of ultrafiltration, an equal volume of buffer used in the enzyme activity assay was added into the protease solution and ultra-filtrated together for 5 min at 4 °C, 12,000 rpm. Protease left on the upper layer of Millipore was collected and diluted to the final concentration of 0.5 μM and enzyme activity was tested. All data were collected from three replicates to obtain average enzymatic activities and error bars.

4.8. Cathepsin L inhibition assay

The inhibition assay of Cathepsin L was performed as previously reported method [41,43]. Briefly, compounds **F8–B6** and **F8–B22** were tested using the commercial Cathepsin L Inhibitor Assay Kit (Abcam, Cat# ab197012). And the known Cathepsin L inhibitor **FF-FMK** was used as the positive compound.

4.9. Cell culture

Vero cells were cultured in (MEM, M&C Gene Technology, Beijing, China) and MDCK cells were cultured in Minimum Essential Medium Dulbecco's modified Eagle's medium (DMEM, M&C Gene Technology, Beijing, China), supplemented with 10% fetal bovine serum (FBS) (PAN Seratech, Aidenbach, Germany) and 100 U/mL penicillin/streptomycin (P/S), and maintained in a humidified atmosphere of 95% air and 5% CO$_2$.

4.10. Cell viability assay

MTT assay was performed to examine the cell viability of the newly identified SARS-CoV-2 M^{pro} inhibitors. Vero and MDCK cells were seeded in 96-well plates. After 18 h incubation, SARS-CoV-2 M^{pro} inhibitors were added to each well. Corresponding vehicles were simultaneously added for blank well. Cell viability was determined 48 h after drug treatment.

4.11. Molecular docking

All of the chemical structures were processed using the *LigPrep* module in Schrödinger 10.2 software (Schrodinger, LLC, NY, USA) [46]. The OPLS3 force field was adopted to perform energy minimization. Default settings were used for all other parameters. The crystallographic structures of the M^{pro} in complex with inhibitors were retrieved from the RCSB Protein Data Bank (PDB) and crystal structures (PDB IDs: 7JUJ) were prepared by the *Protein Preparation Wizard* module in Schrödinger 10.2 software. Default settings were used for all parameters based on the OPLS3 force field. The molecular docking was performed using the *Glide* module with XP (extra precision) in Schrödinger 10.2 software with default settings for all other parameters [47,48].

4.12. Similarity search

The similarity search was performed using Pipeline Pilot 8.5 of Accelrys. The similarities were calculated through the Tanimoto coefficient based on the fingerprint ECFP_6 of each structure. Then, 70 analogs of compound **F8** and 32 analogs of compound **F8–S43** were captured and purchased for biological evaluation.

Declaration of competing interest

The authors declare that they have no known competing financial interests or personal relationships that could have appeared to influence the work reported in this paper.

Acknowledgments

Appendix A. Supplementary data

Supplementary data to this article can be found online at https://doi.org/10.1016/j.ejmech.2022.114508.

Abbreviations used

SARS-CoV-2	severe acute respiratory syndrome coronavirus 2
COVID-19	coronavirus infectious disease 2019
SARS-CoV	severe acute respiratory syndrome coronavirus
MERS-CoV	Middle East respiratory syndrome coronavirus
M^{pro}	Main protease
3CL^{pro}	3-chymotrypsin-like protease
PL^{pro}	papain-like protease
RdRp	RNA-dependent RNA polymerase
FDA	US Food and Drug Administration
CYP3A4	cytochrome P450 3A4
K$_D$	dissociation constant
SPR	surface plasmon resonance
IC$_{50}$	half-maximal inhibitory concentration
SAR	structure-activity relationship;
S2$_C$	S2 channel
HRMS	high-resolution mass spectrometry
PDB	protein data bank
RU	response units
MTT	3-(4,5-dimethylthiazolyl-2)- 2,5-diphenyltetrazolium bromide;
CC$_{50}$	half-maximal cytotoxic concentration
log P	octanol/water partition coefficient

References

[1] N. Zhu, D. Zhang, W. Wang, X. Li, B. Yang, J. Song, X. Zhao, B. Huang, W. Shi, R. Lu, P. Niu, F. Zhan, X. Ma, D. Wang, W. Xu, G. Wu, G.F. Gao, W. Tan, I. China Novel Coronavirus, T. Research, A novel coronavirus from patients with pneumonia in China, 2019, N. Engl. J. Med. 382 (2020) 727–733.

[2] L.T. Phan, T.V. Nguyen, Q.C. Luong, T.V. Nguyen, H.T. Nguyen, H.Q. Le, T. T. Nguyen, T.M. Cao, Q.D. Pham, Importation and human-to-human transmission of a novel coronavirus in Vietnam, N. Engl. J. Med. 382 (2020) 872–874.

[3] C. Wang, P.W. Horby, F.G. Hayden, G.F. Gao, A novel coronavirus outbreak of global health concern, Lancet 395 (2020) 470–473.

[4] M. Dong, E.E. Dando, I. Kotliar, X. Su, B. Dzikovski, J.H. Freed, H. Lin, The asymmetric function of Dph1-Dph2 heterodimer in diphthamide biosynthesis, J. Biol. Inorg. Chem. 24 (2019) 777–782.

[5] G. Li, E. De Clercq, Therapeutic options for the 2019 novel coronavirus (2019-nCoV), Nat. Rev. Drug Discov. 19 (2020) 149–150.

[6] S.A. Amin, T. Jha, Fight against novel coronavirus: a perspective of medicinal chemists, Eur. J. Med. Chem. 201 (2020) 112559.

[7] C. Wu, Y. Liu, Y. Yang, P. Zhang, W. Zhong, Y. Wang, Q. Wang, Y. Xu, M. Li, X. Li, M. Zheng, L. Chen, H. Li, Analysis of therapeutic targets for SARS-CoV-2 and discovery of potential drugs by computational methods, Acta Pharm. Sin. B 10 (2020) 766–788.

[8] C. Gil, T. Ginex, I. Maestro, V. Nozal, L. Barrado-Gil, M.A. Cuesta-Geijo, J. Urquiza, D. Ramirez, C. Alonso, N.E. Campillo, A. Martinez, COVID-19: drug targets and potential treatments, J. Med. Chem. 63 (2020) 12359–12386.

[9] S. Xiu, A. Dick, H. Ju, S. Mirzaie, F. Abdi, S. Cocklin, P. Zhan, X. Liu, Inhibitors of SARS-CoV-2 entry: current and future opportunities, J. Med. Chem. 63 (2020) 12256–12274.

[10] Y. Liu, C. Liang, L. Xin, X. Ren, L. Tian, X. Ju, H. Li, Y. Wang, Q. Zhao, H. Liu, W. Cao, X. Xie, D. Zhang, Y. Wang, Y. Jian, The development of Coronavirus 3C-Like protease (3CL(pro)) inhibitors from 2010 to 2020, Eur. J. Med. Chem. 206 (2020), 112711.

[11] L. Zheng, L. Zhang, J. Huang, K.S. Nandakumar, S. Liu, K. Cheng, Potential treatment methods targeting 2019-nCoV infection, Eur. J. Med. Chem. 205 (2020), 112687.

[12] R. Cannalire, C. Cerchia, A.R. Beccari, F.S. Di Leva, V. Summa, Targeting SARS-CoV-2 proteases and polymerase for COVID-19 treatment: state of the art and future opportunities, J. Med. Chem. (2020), https://doi.org/10.1021/acs.jmedchem.0c01140.

[13] Z. Jin, X. Du, Y. Xu, Y. Deng, M. Liu, Y. Zhao, B. Zhang, X. Li, L. Zhang, C. Peng, Y. Duan, J. Yu, L. Wang, K. Yang, F. Liu, R. Jiang, X. Yang, T. You, X. Liu, X. Yang, F. Bai, H. Liu, X. Liu, L.W. Guddat, W. Xu, G. Xiao, C. Qin, Z. Shi, H. Jiang, Z. Rao, H. Yang, Structure of M(pro) from SARS-CoV-2 and discovery of its inhibitors, Nature 582 (2020) 289–293.

[14] L. Zhang, D. Lin, X. Sun, U. Curth, C. Drosten, L. Sauerhering, S. Becker, K. Rox, R. Hilgenfeld, Crystal structure of SARS-CoV-2 main protease provides a basis for design of improved alpha-ketoamide inhibitors, Science 368 (2020) 409–412.

[15] W. Dai, B. Zhang, X.M. Jiang, H. Su, J. Li, Y. Zhao, X. Xie, Z. Jin, J. Peng, F. Liu, C. Li, Y. Li, F. Bai, H. Wang, X. Cheng, X. Cen, S. Hu, X. Yang, J. Wang, X. Liu, G. Xiao, H. Jiang, Z. Rao, L.K. Zhang, Y. Xu, H. Yang, H. Liu, Structure-based design of antiviral drug candidates targeting the SARS-CoV-2 main protease, Science 368 (2020) 1331–1335.

[16] C. Ma, M.D. Sacco, B. Hurst, J.A. Townsend, Y. Hu, T. Szeto, X. Zhang, B. Tarbet, M.T. Marty, Y. Chen, J. Wang, Boceprevir, GC-376, and calpain inhibitors II, XII inhibit SARS-CoV-2 viral replication by targeting the viral main protease, Cell Res. 30 (2020) 678–692.

[17] L. Fu, F. Ye, Y. Feng, F. Yu, Q. Wang, Y. Wu, C. Zhao, H. Sun, B. Huang, P. Niu, H. Song, Y. Shi, X. Li, W. Tan, J. Qi, G.F. Gao, Both Boceprevir and GC376 efficaciously inhibit SARS-CoV-2 by targeting its main protease, Nat. Commun. 11 (2020) 4417.

[18] M.D. Sacco, C. Ma, P. Lagarias, A. Gao, J.A. Townsend, X. Meng, P. Dube, X. Zhang, Y. Hu, N. Kitamura, B. Hurst, B. Tarbet, M.T. Marty, A. Kolocouris, Y. Xiang, Y. Chen, J. Wang, Structure and inhibition of the SARS-CoV-2 main protease reveals strategy for developing dual inhibitors against M(pro) and cathepsin L, Sci. Adv. 6 (2020), eabe0751.

[19] R.L. Hoffman, R.S. Kania, M.A. Brothers, J.F. Davies, R.A. Ferre, K.S. Gajiwala, M. He, R.J. Hogan, K. Kozminski, L.Y. Li, J.W. Lockner, J. Lou, M.T. Marra, L. J. Mitchell Jr., B.W. Murray, J.A. Nieman, S. Noell, S.P. Planken, T. Rowe, K. Ryan, G.J. Smith 3rd, J.E. Solowiej, C.M. Steppan, B. Taggart, Discovery of Ketone-based covalent inhibitors of coronavirus 3CL proteases for the potential therapeutic treatment of COVID-19, J. Med. Chem. 63 (2020) 12725–12747.

[20] J. Qiao, Y.S. Li, R. Zeng, F.L. Liu, R.H. Luo, C. Huang, Y.F. Wang, J. Zhang, B. Quan, C. Shen, X. Mao, X. Liu, W. Sun, W. Yang, X. Ni, K. Wang, L. Xu, Z.L. Duan, Q. C. Zou, H.L. Zhang, W. Qu, Y.H. Long, M.H. Li, R.C. Yang, X. Liu, J. You, Y. Zhou, R. Yao, W.P. Li, J.M. Liu, P. Chen, Y. Liu, G.F. Lin, X. Yang, J. Zou, L. Li, Y. Hu, G. W. Lu, W.M. Li, Y.Q. Wei, Y.T. Zheng, J. Lei, S. Yang, SARS-CoV-2 M(pro) inhibitors with antiviral activity in a transgenic mouse model, Science 371 (2021) 1374–1378.

[21] D.R. Owen, C.M.N. Allerton, A.S. Anderson, L. Aschenbrenner, M. Avery, S. Berritt, B. Boras, R.D. Cardin, A. Carlo, K.J. Coffman, A. Dantonio, L. Di, H. Eng, R. Ferre, K.S. Gajiwala, S.A. Gibson, S.E. Greasley, B.L. Hurst, E.P. Kadar, A.S. Kalgutkar, J. C. Lee, J. Lee, W. Liu, S.W. Mason, S. Noell, J.J. Novak, R.S. Obach, K. Ogilvie, N. C. Patel, M. Pettersson, D.K. Rai, M.R. Reese, M.F. Sammons, J.G. Sathish, R.S. P. Singh, C.M. Steppan, A.E. Stewart, J.B. Tuttle, L. Updyke, P.R. Verhoest, L. Wei, Q. Yang, Y. Zhu, An oral SARS-CoV-2 M(pro) inhibitor clinical candidate for the treatment of COVID-19, Science 374 (2021) 1586–1593.

[22] Y. Li, W. Li, Z. Xu, Improvement on permeability of cyclic peptide/peptidomimetic: backbone N-Methylation as A useful tool, Mar. Drugs 19 (2021) 311.

[23] N. Qvit, S.J.S. Rubin, T.J. Urban, D. Mochly-Rosen, E.R. Gross, Peptidomimetic therapeutics: scientific approaches and opportunities, Drug Discov. Today 22 (2017) 454–462.

[24] K. Gao, R. Wang, J. Chen, J.J. Tepe, F. Huang, G.-W. Wei, Perspectives on SARS-CoV-2 main protease inhibitors, J. Med. Chem. 64 (2021) 16922–16955.

[25] S.H. Han, C.M. Goins, T. Arya, W.-J. Shin, J. Maw, A. Hooper, D.P. Sonawane, M. R. Porter, B.E. Bannister, R.D. Crouch, A.A. Lindsey, G. Lakatos, S.R. Martinez, J. Alvarado, W.S. Akers, N.S. Wang, J.U. Jung, J.D. Macdonald, S.R. Stauffer, Structure-based optimization of ML300-derived, noncovalent inhibitors targeting the severe acute respiratory syndrome coronavirus 3CL protease (SARS-CoV-2 3CLpro), J. Med. Chem. (2021), https://doi.org/10.1021/acs.jmedchem.1c00598.

[26] C.H. Zhang, E.A. Stone, M. Deshmukh, J.A. Ippolito, M.M. Ghahremanpour, J. Tirado-Rives, K.A. Spasov, S. Zhang, Y. Takeo, S.N. Kudalkar, Z. Liang, F. Isaacs, B. Lindenbach, S.J. Miller, K.S. Anderson, W.L. Jorgensen, Potent noncovalent inhibitors of the main protease of SARS-CoV-2 from molecular sculpting of the drug perampanel guided by free energy perturbation calculations, ACS Cent. Sci. 7 (2021) 467–475.

[27] H.X. Su, S. Yao, W.F. Zhao, M.J. Li, J. Liu, W.J. Shang, H. Xie, C.Q. Ke, H.C. Hu, M. N. Gao, K.Q. Yu, H. Liu, J.S. Shen, W. Tang, L.K. Zhang, G.F. Xiao, L. Ni, D. W. Wang, J.P. Zuo, H.L. Jiang, F. Bai, Y. Wu, Y. Ye, Y.C. Xu, Anti-SARS-CoV-2 activities in vitro of Shuanghuanglian preparations and bioactive ingredients, Acta Pharmacol. Sin. 41 (2020) 1167–1177.

[28] H. Liu, F. Ye, Q. Sun, H. Liang, C. Li, S. Li, R. Lu, B. Huang, W. Tan, L. Lai, Scutellaria baicalensis extract and baicalein inhibit replication of SARS-CoV-2 and its 3C-like protease in vitro, J. Enzym. Inhib. Med. Chem. 36 (2021) 497–503.

[29] P. Liu, H. Liu, Q. Sun, H. Liang, C. Li, X. Deng, Y. Liu, L. Lai, Potent inhibitors of SARS-CoV-2 3C-like protease derived from N-substituted isatin compounds, Eur. J. Med. Chem. 206 (2020), 112702.

[30] N. Drayman, J.K. DeMarco, K.A. Jones, S.A. Azizi, H.M. Froggatt, K. Tan, N. I. Maltseva, S. Chen, V. Nicolaescu, S. Dvorkin, K. Furlong, R.S. Kathayat, M. R. Firpo, V. Mastrodomenico, E.A. Bruce, M.M. Schmidt, R. Jedrzejczak, M. Muñoz-Alía, B. Schuster, V. Nair, K.Y. Han, A. O'Brien, A. Tomatsidou, B. Meyer, M. Vignuzzi, D. Missiakas, J.W. Botten, C.B. Brooke, H. Lee, S.C. Baker, B. C. Mounce, N.S. Heaton, W.E. Severson, K.E. Palmer, B.C. Dickinson, A. Joachimiak, G. Randall, S. Tay, Masitinib is a broad coronavirus 3CL inhibitor that blocks replication of SARS-CoV-2, Science 373 (2021) 931–936.

[31] D.W. Kneller, H. Li, S. Galanie, G. Phillips, A. Labbe, K.L. Weiss, Q. Zhang, M. A. Arnould, A. Clyde, H. Ma, A. Ramanathan, C.B. Jonsson, M.S. Head, L. Coates, J. M. Louis, P.V. Bonnesen, A. Kovalevsky, Structural, electronic, and electrostatic determinants for inhibitor binding to subsites S1 and S2 in SARS-CoV-2 main protease, J. Med. Chem. 64 (2021) 17366–17383.

[32] N. Kitamura, M.D. Sacco, C. Ma, Y. Hu, J.A. Townsend, X. Meng, F. Zhang, X. Zhang, M. Ba, T. Szeto, A. Kukuljac, M.T. Marty, D. Schultz, S. Cherry, Y. Xiang, Y. Chen, J. Wang, Expedited approach toward the rational design of noncovalent SARS-CoV-2 main protease inhibitors, J. Med. Chem. (2021), https://doi.org/10.1021/acs.jmedchem.1c00509.

[33] J. Staron, R. Kurczab, D. Warszycki, G. Satala, M. Krawczyk, R. Bugno, T. Lenda, P. Popik, A.S. Hogendorf, A. Hogendorf, K. Dubiel, M. Matloka, R. Moszczynski-Petkowski, J. Pieczykolan, M. Wieczorek, P. Zajdel, A.J. Bojarski, Virtual screening-driven discovery of dual 5-HT6/5-HT2A receptor ligands with pro-cognitive properties, Eur. J. Med. Chem. 185 (2020), 111857.

[34] W. Yi, C. Dubois, S. Yahiaoui, R. Haudecoeur, C. Belle, H. Song, R. Hardre, M. Reglier, A. Boumendjel, Refinement of arylthiosemicarbazone pharmacophore in inhibition of mushroom tyrosinase, Eur. J. Med. Chem. 46 (2011) 4330–4335.

[35] C. De Monte, S. Carradori, D. Secci, M. D'Ascenzio, P. Guglielmi, A. Mollica, S. Morrone, S. Scarpa, A.M. Agliano, S. Giantulli, I. Silvestri, Synthesis and pharmacological screening of a large library of 1,3,4-thiadiazolines as innovative therapeutic tools for the treatment of prostate cancer and melanoma, Eur. J. Med. Chem. 105 (2015) 245–262.

[36] Y.-L. Su, Z.-Y. Han, Y.-H. Li, L.-Z. Gong, Asymmetric allylation of furfural derivatives: synergistic effect of chiral Ligand and organocatalyst on stereochemical control, ACS Catal. 7 (2017) 7917–7922.

[37] J. Schroder, S. Noack, R.J. Marhofer, J.C. Mottram, G.H. Coombs, P.M. Selzer, Identification of semicarbazones, thiosemicarbazones and triazine nitriles as inhibitors of Leishmania mexicana cysteine protease CPB, PLoS One 8 (2013), e77460.

[38] A. Farjallah, L.R. Chiarelli, M. Forbak, G. Degiacomi, M. Danel, F. Goncalves, C. Carayon, C. Seguin, M. Fumagalli, M. Zahorszka, E. Vega, S. Abid, A. Grzegorzewicz, M. Jackson, A. Peixoto, J. Kordulakova, M.R. Pasca, C. Lherbet, S. Chassaing, A coumarin-based analogue of thiacetazone as dual covalent inhibitor and potential fluorescent Label of HadA in Mycobacterium tuberculosis, ACS Infect. Dis. 7 (2021) 552–565.

[39] Y.S. Xu, J.Z. Chigan, J.Q. Li, H.H. Ding, L.Y. Sun, L. Liu, Z. Hu, K.W. Yang, Hydroxamate and thiosemicarbazone: two highly promising scaffolds for the development of SARS-CoV-2 antivirals, Bioorg. Chem. 124 (2022), 105799.

[40] V. Pandey, K. Sharma, N. Raghav, Ligand-based modeling of semicarbazones and thiosemicarbazones derivatives as Cathepsin B, H, and L inhibitors: a multi-target approach, J. Mol. Struct. 1257 (2022).

[41] A.S. Ashhurst, A.H. Tang, P. Fajtova, M.C. Yoon, A. Aggarwal, M.J. Bedding, A. Stoye, L. Beretta, D. Pwee, A. Drelich, D. Skinner, L. Li, T.D. Meek, J. H. McKerrow, V. Hook, C.T. Tseng, M. Larance, S. Turville, W.H. Gerwick, A. J. O'Donoghue, R.J. Payne, Potent anti-SARS-CoV-2 activity by the natural product Gallinamide A and analogues via inhibition of cathepsin L, J. Med. Chem. 65 (2022) 2956–2970.

[42] M.D. Sacco, C. Ma, P. Lagarias, A. Gao, J.A. Townsend, X. Meng, P. Dube, X. Zhang, Y. Hu, N. Kitamura, B. Hurst, B. Tarbet, M.T. Marty, A. Kolocouris, Y. Xiang, Y. Chen, J. Wang, Structure and inhibition of the SARS-CoV-2 main protease reveal strategy for developing dual inhibitors against M(pro) and cathepsin L, Sci. Adv. 6 (2020).

[43] R. Vicik, M. Busemann, C. Gelhaus, N. Stiefl, J. Scheiber, W. Schmitz, F. Schulz, M. Mladenovic, B. Engels, M. Leippe, K. Baumann, T. Schirmeister, Aziridide-based inhibitors of cathepsin L: synthesis, inhibition activity, and docking studies, ChemMedChem 1 (2006) 1126–1141.

[44] A.F.B. Oleinik, I. T, K. Yu Novitskii, Syntheses based on arylfurans, Khimiya Geterotsiklicheskikh Soedin. 7 (1971) 1011–1013.

[45] A.F.N. Oleinik, K. Yu, L.V. Brattseva, T.A. Gus'kova, G.N. Pershin, A.I. Kravchenko, V.A. Chernov, Synthesis and biological properties of aryloxyfuran, Khim. Farm. Zh. 10 (1976) 65–69.

[46] LigPrep, Schrodinger, LLC, New York, 2015, Version 2.3.

[47] R.A. Friesner, J.L. Banks, R.B. Murphy, T.A. Halgren, J.J. Klicic, D.T. Mainz, M. P. Repasky, E.H. Knoll, M. Shelley, J.K. Perry, D.E. Shaw, P. Francis, P.S. Shenkin, Glide: a new approach for rapid, accurate docking and scoring. 1. Method and assessment of docking accuracy, J. Med. Chem. 47 (2004) 1739–1749.

[48] T.A. Halgren, R.B. Murphy, R.A. Friesner, H.S. Beard, L.L. Frye, W.T. Pollard, J. L. Banks, Glide: a new approach for rapid, accurate docking and scoring. 2. Enrichment factors in database screening, J. Med. Chem. 47 (2004) 1750–1759.